# Photodissociation of group-6 hexacarbonyls: observation of coherent oscillations in an antisymmetric (pseudorotation) vibration in $Mo(CO)_5$ and $W(CO)_5$

**Kyriaki Kosma,*† Sergei A. Trushin, Werner Fuß,* Wolfram E. Schmid and Brigitte M. R. Schneider**

*Received 28th May 2010, Accepted 5th August 2010*
**DOI: 10.1039/c0cp00731e**



On dissociation of $M(CO)_6$, M = Cr, Mo and W, by a femtosecond UV laser (<270 to 360 nm), pronounced coherent oscillations are observed in the pentacarbonyl products on probing by long-wavelength (810 nm) ionization in the gas phase. They are vibrations in the ground state, driven by the slope from a conical intersection on relaxation from the initially formed excited state ($S_1$). Surprisingly, with M = Mo and W we also find a fundamental of an antisymmetric ($b_2$ in $C_{4v}$) vibration. From positive and negative displacements along such a coordinate one would expect the same signal, so that there should be only overtones. Vibrational selection rules are therefore considered for time-resolved spectroscopy. The reason for the symmetry breaking is suggested to result from the fact that the phase in superposition of wave functions is established by the pump process and this phase is conserved in probing, independently of the probe delay. An antisymmetric fundamental can be observed, if there is a small tunneling splitting in a state involved in the probe process. The observations also imply some conclusions on the dissociation and relaxation processes and the potentials: with longer wavelengths, the wave packet enters on the same surface but from a different direction to $S_1$. Only a very minor fraction of the available energy appears as coherent oscillation. There is no equipartition at the end, and a second CO is cleaved off in few picoseconds, even if there is only very little excess energy. Triplets do not contribute, even in the tungsten system and at longest wavelengths. The dissociation mechanism involves passage of the wave packet from all initial states over an avoided crossing to a repulsive ligand-field surface. It predicts that in some other molecules, the barrier caused thereby is larger and for long photolysis wavelength the lifetime is long enough for intersystem crossing to take place; it also predicts wavelength dependences in these cases. It is again emphasized that there is no vertical internal conversion; instead, the molecule is controlled by slopes and intersections of potentials. Also lifetimes can be considered as a control parameter in photochemistry.

## 1. Introduction

The photodissociation of the hexacarbonyls of group-6 transition metals is the prototype of the photochemistry of other metal carbonyls and organometallic photoreactions. The compounds eliminate a single CO,[1,2] and the resulting unsaturated complexes can serve as models for species that are catalytically active *e.g.* in CH activation.[3] Two groups of transitions are expected in the near UV:

(1) those involving d → d excitation (''ligand field'', LF, or ''metal centered'', MC). The highest occupied and the lowest unoccupied orbitals are of d type. As all d → d transitions they are expected to be weak.[4] The LF excited states are directly repulsive.

(2) the d → π* metal-to-ligand charge-transfer (MLCT) transitions. Those which are symmetry-allowed ($T_{1u}$ in the octahedral hexacarbonyls) are very intense. Because the MLCT states correlate with charge-separated fragments, they are not expected to be dissociative.

Since the work of the Baerends[5–7] and Pierloot[8] groups it is known that the MLCT states lie below most of the LF states in the group-6 carbonyls $M(CO)_6$. This is also confirmed in the more recent work of the Daniel group on $Cr(CO)_6$.[9,10] The calculations[5,6,10] furthermore suggest that on stretching a single M–C bond from one of the lowest MLCT states ($T_{2u}$) the population can flow *via* an avoided crossing to an LF surface, which steeply declines from higher energy down to (the first excited state of) the dissociation product $M(CO)_5$; but the other MLCT states rise along this coordinate and thus seem not dissociative[5,6] or lead to higher excited states of the product.[5,6,10]

In time-resolved experiments with excitation mainly near 270 nm and probing by nonresonant (800 nm) photoionization of $M(CO)_6$ (M = Cr, Mo, W),[11–13] $Fe(CO)_5$,[14] $Ni(CO)_4$[15] and other carbonyls[16] we found previously that the molecules indeed do not directly dissociate from the $T_{1u}$ and other MLCT states but change the electronic state before. The dissociation product $M(CO)_{n-1}$ initially appears in its first

*Max-Planck-Institut für Quantenoptik, Hans-Kopfermann-Str. 1, D-85748 Garching, Germany. E-mail: kosma@iesl.forth.gr, w.fuss@mpq.mpg.de*
† Current address: Institute of Electronic Structure and Laser, Foundation for Research and Technology, P.O. Box 1527, 71110 Heraklion, Greece.

excited singlet state $S_1$; from there, the unsaturated carbonyls of coordination numbers 5 and 4 relax along a pseudorotation coordinate through a Jahn–Teller induced conical intersection to $S_0$. (Those with threefold coordination fluoresce or phosphoresce instead.[15]) In this state pronounced coherent oscillations along this coordinate are observed in $M(CO)_5$ (M = Cr, Mo, W)[11–13] and similarly with some dinuclear carbonyls.[16] The relaxation pathway from $Cr(CO)_6$ down to the $S_0$ of $Cr(CO)_5$ and the oscillations on these surfaces have been investigated by Paterson *et al.* by trajectory and wavepacket dynamics calculations,[17,18] which confirmed the basic mechanism. Very recently Long reviewed these experiments and calculations and summarized conclusions on the mechanism.[19]

In this work we focus on these coherent oscillations in the dissociation product, in particular in $Mo(CO)_5$. Remarkably, one of them corresponds to the fundamental of an antisymmetric ($b_2$ in $C_{4v}$) vibration; in $Cr(CO)_5$, it was not found with certainty.[13] Selection rules for time-resolved spectroscopy are therefore derived in Section 4.3. These (late) oscillations also provide us some conclusions on the early path, the potentials of $M(CO)_6$ and $M(CO)_5$, and the relaxation mechanism (Section 4.4–4.6).

## 2. Experiments and calculations

The experiments were performed in the setup of our preceding work,[13] however, using only the UV pulses with duration of 28 fs (at 350–360 nm: 42 fs), not the shorter ones (10 fs). Briefly, $M(CO)_6$ was excited in the gas phase (pressure $10^{-4}$ to $10^{-7}$ mbar, background $10^{-9}$ mbar) by weak femtosecond UV pulses ($10^9$ W cm$^{-2}$, 25 μJ cm$^{-2}$), tuned in the range 270–360 nm, and then after variable delay probed by nonresonant ionization ($10^{13}$ W cm$^{-2}$, 810 nm, ~17 fs); the signals are the yields of the parent and fragment ions $M(CO)_n^+$ determined in a time-of-flight mass spectrometer as functions of the delay time. The time zero was taken from the maximum of the $Xe^+$ signal from Xe added in all measurements. For M = Mo and W we measured the ion signals $M(CO)_6^+$ and $M(CO)_5^+$, for M = Mo also $Mo(CO)_4^+$. With the UV and IR pulse durations used, the time resolution (width of the instrumental function, *i.e.*, the correlation of the pump with the *p*-th power of the probe, where $p \geq 3$ is the order of ionization) is 30 fs (43 fs at the longer wavelengths).

The generation of the 10–17 fs 810 nm pulses is reported in ref. 20 and 21, that of the tunable 28-fs UV pulses in ref. 21. Briefly, we shortened the pulses (810 nm, 45 fs, 1 kHz) of a commercial Ti–sapphire laser system, by focusing ($f$ = 2 m) 1 mJ of them into a cell (length 1.5 m, equipped with quartz-glass windows of 0.2 mm thickness) filled with 200 mbar Ar + 800 mbar He (instead of atmospheric-pressure of Ar as in ref. 20). Under these conditions the pulses are broadened by self-phase modulated and acquire a chirp, which can be used to compress the pulses to 17 fs (determined by a commercial autocorrelator) by reflection from chirped mirrors.[20,21] Using 1 bar of Ar instead of the gas mix gives rise to a pulse duration of 10 fs.[20] Part (~10 μJ) of this radiation (17 fs) is used for probing.

Another part (0.8 mJ) served for the generation of the UV (pump) wavelengths. In most cases they were isolated by dielectric mirrors from a supercontinuum generated in another gas cell. For this purpose, the 810 nm 17 fs radiation is limited by a diaphragm in diameter (to 4 mm) and energy (to 0.4 mJ) and refocused ($f$ = 1 m) into atmospheric-pressure Ar. With a beam path in air and recompression by a pair of $CaF_2$ prisms, we obtained tunable UV pulses with durations in the ionization chamber of 28 fs; the duration is limited by higher-order dispersion. The spectral width was limited by a diaphragm between the prisms to 9 nm. The weak absorption in the long-wavelength wing of the carbonyls required a stronger pump pulse at 350 and 360 nm. For this purpose we used the radiation generated in a commercial (TOPAS, Light Conversion) optical parametric generator combined with various nonlinear frequency conversion steps, as previously (*e.g.* ref. 22). It delivered pulses of a few μJ with durations of 42 fs after a prism compressor. In a few experiments we also used the third harmonic (270 nm, 28 fs) generated in a short Ar cell (see ref. 13 and 21 for details).

As mentioned, the other part (~10 μJ) of the radiation, taken aside before UV generation, was used for probing. The probe delay was varied in steps of 3.3 fs (2 × 0.5 μm). Both beams were combined before the ionization setup by a mirror with a hole. Pump and probe pulses are focused by mirrors (focal lengths 1 and 0.7 m, respectively) into the ionization region of the mass spectrometer.

Pump and probe lasers were linearly polarized with parallel orientation. In our previous work, rotational or polarization effects could not be detected.[11,12]

In the calculations, we first optimized the geometry of $Cr(CO)_5$ and $Mo(CO)_5$, and then calculated the vibrations by density functional theory using DFT/B3PW91 in the Gaussian03 package.[23] As basis set we chose 6-311G(d) for C and O and the pseudo potential LANL2-DZ for Cr and Mo.[24] A correction factor was not applied to the calculated vibrational wavenumbers.

## 3. Results

### 3.1 UV spectra

Fig. 1 shows the gas-phase UV spectra of the three $M(CO)_6$ measured with saturated vapor in 1 and 10 cm cells as in ref. 13. Absorption cross sections were calibrated by the solution values.[25,26] The figure also indicates the pump wavelengths used for $Mo(CO)_6$ and $W(CO)_6$ and the location of the states of the MLCT (u symmetry) and LF (g symmetry) groups, as predicted by recent high-level calculations for the chromium compound.[9,10] The three spectra are very similar. The pump wavelength 286 nm excites the longest-wavelength allowed transition ($T_{1u}$) of $M(CO)_6$, those at 270 nm and 303 nm are still in the wing of this band, whereas the other wavelengths are in the precursor bands, all of MLCT type.

### 3.2 Time-resolved data of $Mo(CO)_6$

In the time-resolved measurements we only investigated the ions $M(CO)_n^+$ with $n$ = 6, 5, 4, because the lighter fragments seemed not to contain additional information. Examples of time-dependent signals are shown in Fig. 2–10. As in our

 

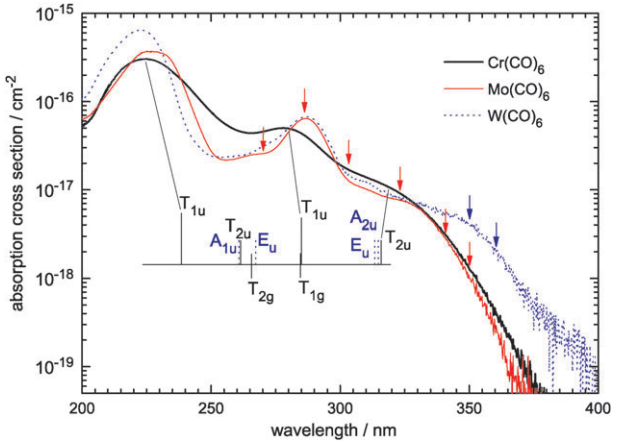


**Fig. 1** Gas-phase UV spectra of the three hexacarbonyls. The assignment for $Cr(CO)_6$ is based on the calculations of Villaume *et al.*,[10] with some states (dotted lines) taken from a previous work of the same group.[9] Vertical arrows indicate the wavelengths used for $Mo(CO)_6$ and $W(CO)_6$.

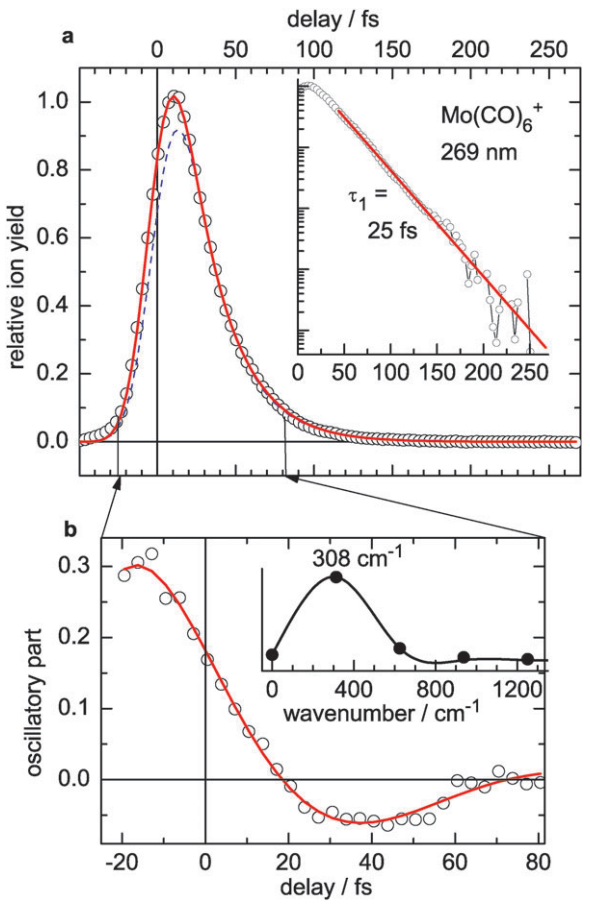


**Fig. 2** Parent ion signal on exciting molybdenum carbonyl at 269 nm. The dashed line in part (a) is a simulation by a single exponential fitted to the tail (see the logarithmic inset) and extrapolated back to earlier times, with convolution with the instrumental function. Dividing the data by this curve and subtracting 1 results in the oscillatory part (b), whose Fourier transform is shown in the inset. The solid line in (a) is a simulation by the exponential decay and this oscillation.

previous work (see, *e.g.*, ref. 13), the signals were simulated by sums of exponentials (each with a time constant $\tau_i$ as parameter), convoluted with the instrumental function (*i.e.*, the correlation of the pump pulse with the $p$-th power of the probe, where $p$ is the order of ionization); if an oscillatory modulation was visible, these simulation functions were multiplied by one or more periodic functions of the type

$$f_{\mathrm{osc}} = 1 + A \exp(-t/\tau_{\mathrm{deph}}) \cos(2\pi t/\tau_{\mathrm{osc}} - \phi) \qquad (1)$$

(see ref. 13) with the amplitude $A$, the (pure) dephasing time $\tau_{\mathrm{deph}}$, the period $\tau_{\mathrm{osc}}$ and the phase $\phi$ as parameters. Instead of $\tau_{\mathrm{osc}}$, below we give the wavenumbers $c/\tau_{\mathrm{osc}}$, because the oscillations are interpreted as vibrations.

The time constants $\tau_i$ are interpreted as lifetimes of the population that passes consecutively through locations $L_i$ on the potential surfaces; these locations differ in their mass spectra, with fragmentation increasing with $i$. This is because more and more electronic energy is converted to kinetic energy of the nuclei, which after ionization causes dissociation of the ion; *i.e.*, a hot neutral gives rise to a hot ion, which tends to more fragmentation. Thus in the Franck–Condon region ($L_1$) one observes only the parent ion (Fig. 2 and 3). But already in $L_2$ (which has more excess energy than $L_1$), $M(CO)_6^+$ is not observed anymore. Therefore the $L_1$ signal decays singly exponentially with $\tau_1$, whereas the $M(CO)_5^+$ signal rises with $\tau_1$ and in its decay shows $\tau_2$. Because with M = Mo and W (not with the chromium compound) this signal is also observed from $L_3$ and $L_4$, one can find in its decaying part also $\tau_3$ and $\tau_4$ (Fig. 4; earlier part not shown in detail). But they appear with better signal-to-noise ratio in the $M(CO)_4^+$ fragment.

The signals coming from more than one $L_i$ are composed of several exponentials. These contributions are shown, together

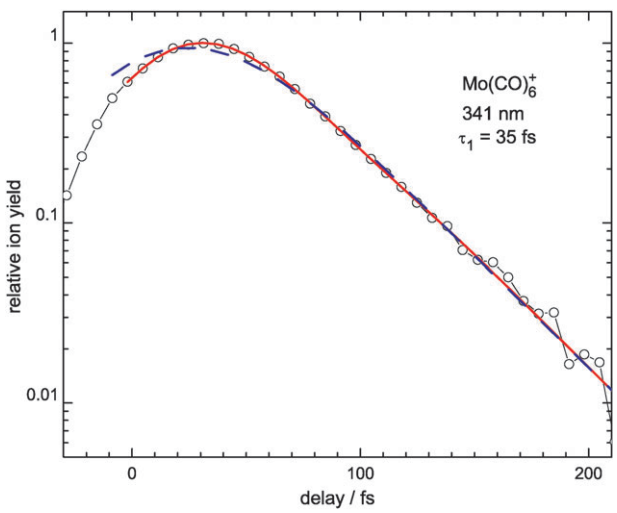


**Fig. 3** Parent ion signal $Mo(CO)_6^+$ on exciting molybdenum carbonyl at 341 nm. A procedure as in the preceding figure reveals slight deviations at early times from a singly exponential decay (with convolution, broken line), which can be simulated by an oscillation of wavenumber 275 cm$^{-1}$. The solid line represents the combined simulation.

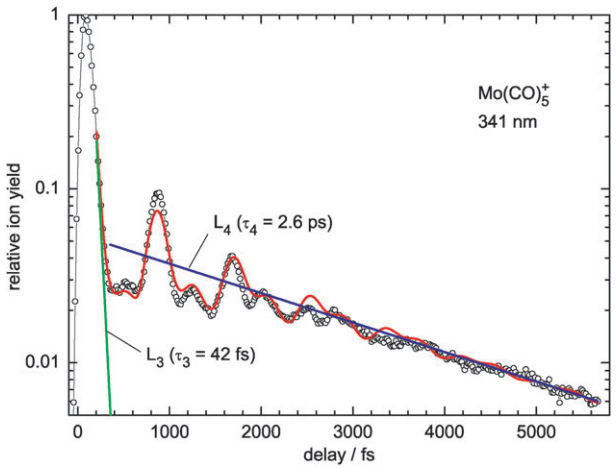


**Fig. 4** Fragment ion signal $Mo(CO)_5^+$ on exciting molybdenum carbonyl at 341 nm. The open symbols show the data after subtraction of their asymptotic value (0.002) at long time. (The $Mo(CO)_5^+$ signal should decay to 0, because according to the Discussion, $\tau_4$ is the time for dissociation of $Mo(CO)_5$; the pedestal of 0.002 might represent the small fraction of molecules that have not enough excess energy to split off a second CO: in fact, at 350 nm, it is slightly larger: 0.0026.) The straight lines show the exponential parts $L_3$ and $L_4$ of the simulation, whereas the curves also include the oscillatory part.

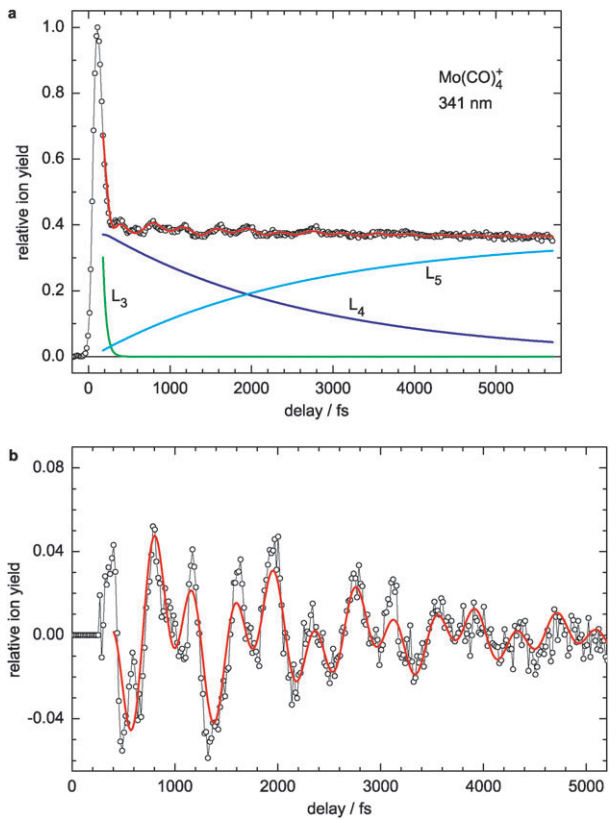


**Fig. 5** The $Mo(CO)_4^+$ signal (open symbols in a) on exciting molybdenum carbonyl at 341 nm. In a first step, the data are simulated by a sum of exponentials, whose terms $L_3$ (decaying with $\tau_3$), $L_4$ ($\tau_4$) and $L_5$ (rising with $\tau_4$) are shown. Subtracting $L_3$ and $L_5$, dividing by $L_4$ and subtracting 1 results in the oscillatory part shown in b. The simulation curve in a includes exponential and oscillatory parts.

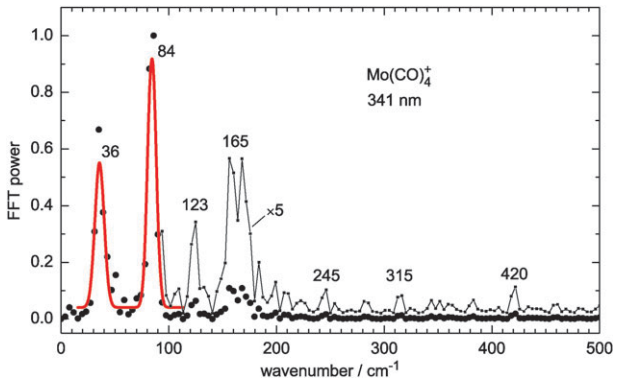


**Fig. 6** Fourier transform of the oscillatory part shown in Fig. 5b. Data at higher wavenumbers are also shown five times magnified.

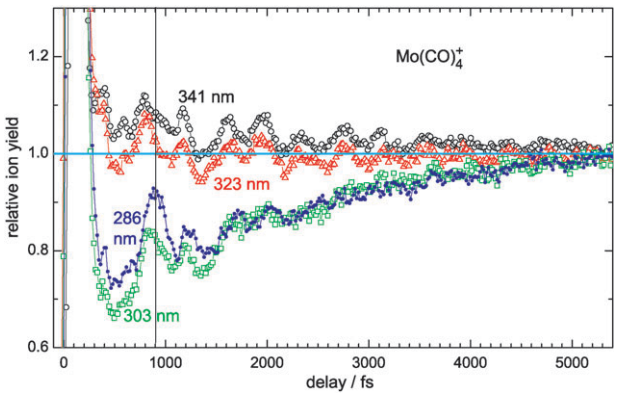


**Fig. 7** Comparison of the oscillatory parts of the $Mo(CO)_4^+$ signals using different pump wavelengths. The first maximum of the oscillation appears earlier at longer pump wavelengths.

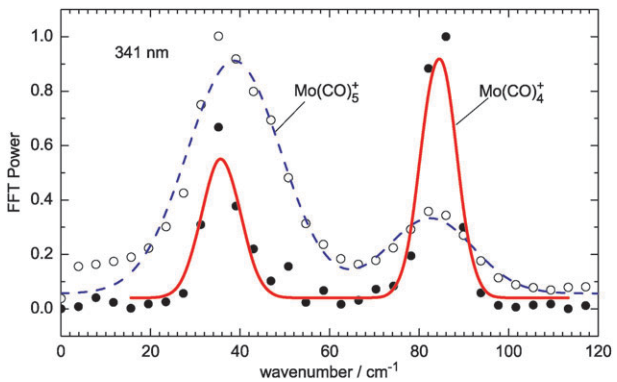


**Fig. 8** Fourier transforms of the oscillatory parts of the $Mo(CO)_5^+$ and $Mo(CO)_4^+$ signals. The relative amplitudes differ.

with the original signal, in Fig. 4 and 5a as examples. Besides the exponential part, these examples also show some oscillations in the signal. Whereas the exponentials represent the decay of the population, oscillations are generally interpreted as a vibration, which modulates the probe transition probability (not the population) in a certain $L_i$ ($L_4$ in the examples). The oscillatory part is isolated from the original signal in Fig. 5a by subtracting the $L_3$ and $L_5$ parts and dividing by the

 

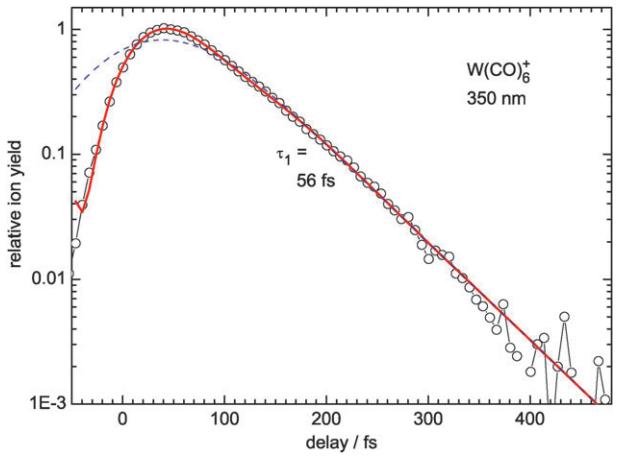


**Fig. 9** Parent ion signal $W(CO)_6^+$ (open symbols) on exciting tungsten carbonyl at 350 nm. The broken line is an exponential simulation of the late part, back-extrapolated with convolution. The solid line includes also a highly damped early oscillation. See Fig. 2 for the further procedure.

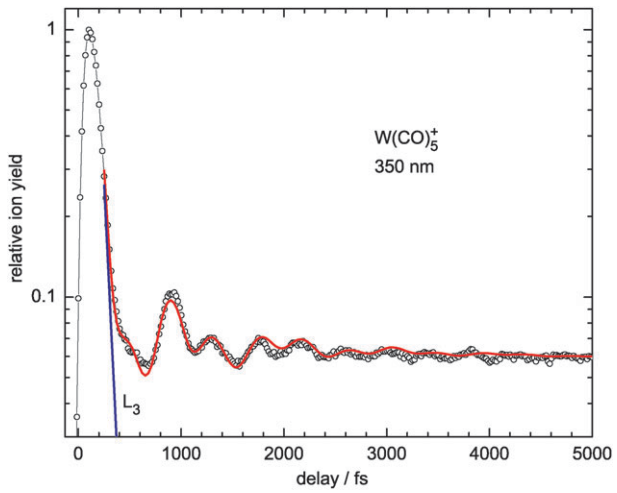


**Fig. 10** The $W(CO)_5^+$ signal (open symbols) on exciting tungsten carbonyl at 350 nm. On subtracting the $L_3$ decay, the result shows directly the oscillatory part of $L_4$. The solid line is a simulation with two oscillation frequencies, including also the $\tau_3$ exponential.

$L_4$ exponential. (For Fig. 4, the procedure is the same, the $L_5$ contribution being 0, however.) The result should be a product of functions $f_{osc}$ of type (1). It is shown (after subtracting 1) in Fig. 5b (open symbols). The solid line is a simulation with the product of two $f_{osc}$ (wavenumbers 36 and 84 $cm^{-1}$). The sharp structures at the early times indicate that the data also contain higher frequencies. Indeed in the Fourier transform (Fig. 6) of this oscillatory part one observes higher frequencies. From the data alone, we cannot tell which of the higher-frequency peaks is still real; however, a plausible assignment will be given in Section 4.2.

We interpret also data from the Franck–Condon (FC) region on pumping at 269 and 341 nm with a contribution by an oscillation: on extrapolating the exponential decay of the $Mo(CO)_6^+$ signal (inset in Fig. 2a) back to early times (dashed line in Fig. 2a), the data show a deviation, which can be satisfactorily fitted by a preceding shorter-time decay, but slightly better by a highly damped oscillation. It is separately shown in Fig. 2b. Due to its rapid damping, its wavenumber is not very accurate. In the same way, the $Mo(CO)_6^+$ data at 341 nm can be simulated: in Fig. 3, the broken line shows an exponential fit, extrapolated back to early times, whereas the solid line also includes the oscillation. We should mention that in the FC region the assumption of a highly damped oscillation is only an interpretation; it is motivated by the fact that in $Cr(CO)_6$ it appears clearly.[13] The $Mo(CO)_6$ and $W(CO)_6$ data could alternatively be simulated by an additional time constant, in particular, if the time resolution was worse (as it was in the early work[12]).

The simulation of the oscillations also yields the dephasing times (listed below) and the phases. The latter reflect the times, when the oscillation appears. These times can be more directly visualized by Fig. 7, which shows that the first prominent maximum moves systematically to shorter delay, the longer is the pump wavelength. One can also recognize that the frequencies and amplitudes do not visibly depend on the wavelength, whereas the damping seems to be faster with higher energy of the pump photon; as it turns out in the evaluation, this damping is caused by the wavelength dependence of $\tau_4$ (listed below) whereas the pure dephasing time seems practically constant. Although the phases vary to some extent, the wavenumbers are the same (within about $\pm 2$ $cm^{-1}$) for all wavelengths. This shows that they are due to vibrations in the same species and state ($S_0$ of $Mo(CO)_5$, Section 4.2), independently of the pump wavelength.

Comparing different fragment signals at a given wavelength, it turns out that the oscillations coincide in the frequencies and phases, which confirms that all these oscillating fragment ion signals are due to the same neutral species and state. However, the relative amplitudes can differ between the fragment signals, as shown in Fig. 7. The phenomenon is attributed in Section 4.4 to an additional resonance in the probing process.

Because the time-resolved data of $Mo(CO)_4^+$ are more intense, have a better signal-to-noise ratio and show sharper structures than those of $Mo(CO)_5^+$, the Fourier transform bands are narrower (with more accurate wave numbers), and higher frequencies seem to emerge from the background (Fig. 6).

The time constants and oscillation data resulting from the evaluation are compiled in Tables 1 and 2. The former were

**Table 1** Time constants observed for $Mo(CO)_6$ and $W(CO)_6$ at different pump wavelengths

| | $\tau_1$/fs | $\tau_2$/fs | $\tau_3$/fs | $\tau_4$/ps |
|---|---|---|---|---|
| $Mo(CO)_6$ | | | | |
| 267–270 nm[12] | 30 ± 1 | 35 ± 2[b] | 56 ± 5[b] | 1.0 ± 0.2[b] |
| | 26[13] | | | |
| 286 nm | 26 | 35 | 56 | 1.45 |
| 303 nm | | | 56 | 1.56 |
| 323 | | | (42)[a] | 1.82 |
| 341 nm | 35 | 33 | 42 | 2.6 |
| 350 nm | | | (42)[a] | 3.0 |
| $W(CO)_6$ | | | | |
| 267 nm[12] | 46 ± 1 | 30 ± 2[b] | 70 ± 5[b] | 1.15 ± 0.2[b] |
| 350 nm, 360 nm | 58–60 | | 55 | ∞ |

[a] Taken over from 341 nm. [b] Denoted $\tau_3$, $\tau_4$, $\tau_5$ in ref. 12, see ref. 13.

**Table 2** Wavenumbers $\nu$ and dephasing times $\tau_{deph}$ of oscillations observed in the Franck–Condon region of $M(CO)_6$ and the dissociation products $M(CO)_5$ (observation regions $L_1$ and $L_4$ of $M(CO)_6$, M = Mo and W) at different pump wavelengths

| | $\nu_a$/cm$^{-1}$ | $\nu_b$/cm$^{-1}$ | $\tau_{deph}$ |
|---|---|---|---|
| $Mo(CO)_6$/269 nm | 308 (+100, −50)[a] | | 33 fs |
| $Mo(CO)_6$/341 nm | 275 (+100, −50)[a] | | 64 fs |
| $Mo(CO)_5$/269–350 nm | 83.6 ± 1.2[b] | 36.0 ± 1.4[b] | 1.0–1.5 ps |
| $Mo(CO)_5$/267 nm[12] | 84.2 | Visible | |
| $W(CO)_6$/350 nm | 230 (+100, −50)[a] | | 60 fs |
| $W(CO)_5$/350, 360 nm | 79.0 ± 0.5[c] | 32.0 ± 1.5[c] | 1.0–1.5 ps |
| $W(CO)_5$/267 nm[12] | 79.7 | | |

[a] Estimated error limit; it is large, because dephasing times and population lifetimes ($\tau_{deph}$ and $\tau_1$) are shorter than a period. [b] Standard deviation on averaging results from 14 data sets in the given wavelength range. [c] Standard deviation (probably underestimated) on averaging 3 values.

only investigated as far as necessary to extract the late oscillations, on which the present work is focused. Therefore the time constants are less accurate (due to less statistics) and less complete than in our previous investigations (*e.g.* ref. 13), some of them even only taken over from those at a different pump wavelength. A rough evaluation mainly of $\tau_3$ and $\tau_4$ was necessary to extract the oscillations. But one can anyway recognize some trends that are similar to the observations for $Cr(CO)_6$.[13]

Obviously $\tau_1$ is slightly lengthened at longer wavelengths, whereas $\tau_2$ is practically not affected. Remarkably $\tau_3$ becomes shorter with smaller excess energy (longer pump wavelengths), whereas $\tau_4$ becomes longer. The latter observation confirms the previous assignment of $\tau_4$ to the endothermic elimination of a second CO from the hot ground state of the primary product $M(CO)_5$, because the longer wavelength provides less excess energy. It is further supported by the value $\tau_4 = \infty$ for $W(CO)_6$ at 350–360 nm, because in this case there is in fact not enough energy for this dissociation step (see the energies at the end of Section 4.1).

The dephasing times (which were only roughly determined) seem not to vary much. The wavelength dependence of the oscillation decay, that is visible in Fig. 7, is caused by the varying population decay times ($\tau_4$), not by $\tau_{deph}$.

### 3.3 Time-resolved measurements of $W(CO)_6$

For tungsten carbonyl we measured data only at 350 and 360 nm, in the long-wavelength tail of the UV spectrum, to compare them with the previous data at 267 nm. The results are also given in Tables 1 and 2, and two examples of the time-resolved data are shown in Fig. 9 and 10. The parent ion (Fig. 9) is again interpreted by a singly exponential decay (back-extrapolation shown by the dashed line in the figure) superimposed by a rapidly damped oscillation. After an initial decay with $\tau_2$ and $\tau_3$, the $W(CO)_5^+$ fragment signal (Fig. 10) oscillates around a constant value, so that extraction of the oscillatory part is simpler than in the molybdenum case. The lack of further decay (implying $\tau_4 = \infty$) is in contrast to the decay of $Mo(CO)_5^+$ (time constant $\tau_4 = 2.6$ ps at 341 nm). As already mentioned above, it indicates that elimination of a second CO (as from the molybdenum and chromium carbonyls) does not take place with $W(CO)_6$ at long wavelengths, because the energy is not sufficient.

### 3.4 Calculation of the $M(CO)_5$ vibrations

Already previously,[11–13] we assigned the oscillations with wavenumber 80–100 cm$^{-1}$ observed in the observation window $L_4$ (*i.e.* during the $\tau_4$ decay) of $M(CO)_6$ to pseudorotation in the ground state of the dissociation product $M(CO)_5$. This was consistent with the general frequency range of CMC bending vibrations and provided us a plausible interpretation in terms of the path on the potentials. It was further confirmed by the trajectory and quantum dynamical calculations of Paterson *et al.*[17,18] In order also to identify the newly observed low frequency (near 35 cm$^{-1}$) in the molybdenum and tungsten systems, we calculated the vibrations of $M(CO)_5$ (M = Cr and Mo) in the ground singlet ($S_0$, in the calculated $C_{4v}$ equilibrium geometry) and triplet ($T_0$, in the calculated $D_{3h}$ equilibrium geometry) states by density-functional theory (Tables 3 and 4). The (trigonal bipyramidal) $T_0$ minimum of $Cr(CO)_5$ is found to be higher than the (square pyramidal) $S_0$ minimum by 0.455 eV, similarly as in recent calculations.[27] The values for the CO stretch wavenumbers are well consistent with other calculations of these vibrations.[27,28] For a quality check of the lower frequencies, we applied the calculation also to the parent compound $Cr(CO)_6$ and found that they agree with the experimental ones[29] within <10% (most of them within <5%).

In Table 3 we italicize the wavenumbers assigned in Section 4.2 to those observed in the time-resolved measurements. The tables also give the symmetries and types of vibrations.

**Table 3** Vibrations (wavenumbers in cm$^{-1}$) of $Cr(CO)_5$ and $Mo(CO)_5$ in the singlet ground state ($S_0$) in equilibrium geometry (square pyramid, $C_{4v}$), calculated by density functional theory (without correction factor). The first four are illustrated in Section 4.2

| Symmetry | Type | $Cr(CO)_5$ | $Mo(CO)_5$ |
|---|---|---|---|
| $b_2$ | CMC | 49 | *51.2* |
| e | CMC planar + axial | 75 | 70.4 |
| $b_1$ | CMC planar | 89.7 | 83.2 |
| $a_1$ | CMC umbrella | *96.6* | *86.6* |
| e | CMC axial | 99 | 91.8 |
| e | MCO | 312.2 | 306.4 |
| $a_2$ | MCO | 315 | 296.8 |
| $b_2$ | MC equatorial | 414.2 | 398.9 |
| $a_1$ | MC equ. − axial | *415.1* | *410.7* |
| e | MCO | 461 | 391 |
| $a_1$ | $MC_{ax}$ + MCO | 476.1 | 476.3 |
| $b_2$ | MCO | 487.2 | 484.5 |
| e | MCO planar | 538 | 507 |
| $b_1$ | MCO planar | 540.6 | 466.9 |
| e | MC equatorial | 652.3 | 557.7 |
| $a_1$ | $MC_{ax}$ + MCO | 672.7 | 594.8 |
| e | CO | 2074.3 | 2060.4 |
| $a_1$ | CO | 2080.7 | 2059.2 |
| $b_2$ | CO | 2093.2 | 2080.7 |
| $a_1$ | CO | 2131.6 | 2115.6 |

Nomenclature: $b_1/b_2$ is symmetric/antisymmetric to the plane bisecting the 90°-CMC angle. (In some literature, it is the other way around.) In the column "type", a stretch vibration is indicated by two atoms and a bending vibration by three atoms.

 

**Table 4** Vibrations (wavenumbers in $cm^{-1}$) of $Cr(CO)_5$ in the lowest triplet state ($T_0$) in equilibrium geometry (trigonal bipyramid, $D_{3h}$), calculated by density functional theory (without correction factor)

| Symmetry | Character | $Cr(CO)_5$ |
|---|---|---|
| e′ | CMC | 44.6 |
| e″ | CMC | 76 |
| $a_2''$ | CMC | 78.1 |
| e′ | CMC | 94.2 |
| $a_2'$ | MCO | 282.1 |
| e″ | MCO | 306.6 |
| e′ | MCO | 342.7 |
| $a_1'$ | MC | 364 |
| $a_2''$ | MC + MCO | 392.2 |
| $a_1'$ | MC | 413.3 |
| e′ | MC + MCO | 447.6 |
| e″ | MCO | 420.6 |
| $a_2''$ | MC + MCO | 556.5 |
| e′ | MC + MCO | 610.4 |
| e′ | CO | 2056.8 |
| $a_1'$ | CO | 2066 |
| $a_2''$ | CO | 2083.1 |
| $a_1'$ | CO | 2121.7 |

## 4. Discussion

### 4.1 The dissociation path

Here we briefly summarize the ideas on the dissociation path that were derived from our previous measurements on group-6 hexacarbonyls and from other investigations.[11–13] (Many details are also reported in the recent mechanistic summary.[19]) We also present some refinements prompted by the recent calculations of Villaume *et al.*[10]

As shown schematically in Fig. 11 (see also ref. 13), excitation leads to an MLCT state; the corresponding absorption bands are broad (Fig. 1), overlapping with each other, and are more intense than LF bands.[4] From each populated state the molecules reach directly (*i.e.*, without preceding vertical relaxation) the repulsive surface of the lowest LF state, where the actual dissociation (extension of the M–CO bond) takes place. But the paths are still separate (details are given in Fig. 13 and context in Section 4.6), merging only in $S_1$ of the dissociation product $M(CO)_5$. From there, the molecules pass through a JT-induced CI with a trigonal-bipyramidal ($D_{3h}$) structure to an $S_0$ minimum with a square-pyramidal ($C_{4v}$) structure. This last relaxation corresponds to a single step of pseudorotation (exchange of the ligand vacancy with an adjacent substituent). Actually with short pump wavelength the path from the CI first leads to a saddle point, from where then one of the minima is reached (inset in Fig. 11). The slope down from the CI stimulates coherent oscillations in a minimum. The probing detects the radial component of them, because in this direction the transition energy is tuned from 2.0 eV ($Cr(CO)_5$) or 2.6 eV ($Mo(CO)_5$) to 0 (probe photon 1.53 eV; see the energetics at the end of this section). The radial component is an e′ bending (in $D_{3h}$) of the equatorial ligands (scheme at the abscissa of Fig. 11; other details in ref. 12).

The transition from the MLCT states to the LF surface is not detailed in Fig. 11. It was suggested in ref. 13 to take place *via* conical intersections between the MLCT surfaces with the LF surface, or more precisely, around the lower cone of such

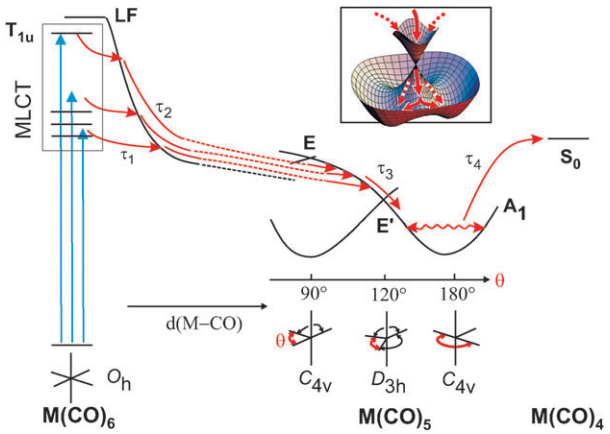


**Fig. 11** Schematic potentials and dynamics, using three different pump wavelengths which initially excite MLCT states. The initial relaxation (during slightly different times $\tau_1$) follows MC stretch and JT active coordinates on the MLCT potentials, from where the wave packet crosses over to the lowest LF surface. On this surface, the trajectories are still separate (during $\tau_2$), merging only above the conical intersection (CI) in the dissociation product $M(CO)_5$. During $\tau_2$, the MC distance increases much less than indicated for clarity in the figure (broken lines). After passing the CI (within $\tau_3$), the wave packet oscillates in the $C_{4v}$ minima along the pseudorotation coordinates indicated at the bottom; there are three symmetry-equivalent minima of this kind around each $D_{3h}$ CI (inset), and each minimum has two symmetry-equivalent such CIs as neighbors, which can both be reached from $S_1$ (only one CI shown). At short pump wavelengths (286 nm), the wave packet enters into the funnel along a ridge or cusp line, at long wavelengths (341 nm) along a valley (dotted arrows in the inset, see text). Note that the same minima are reached at both wavelengths. Further dissociation to $M(CO)_4$ (within $\tau_4$) is promoted by excess energy; with $W(CO)_6$ at 350 and 360 nm, this process does not take place (*i.e.*, $\tau_4 = \infty$) due to lack of excess energy.

an intersection, where the crossing is avoided. In the meantime, Villaume *et al.* presented for M = Cr a new high-level calculation on the potentials resulting, if one M–CO bond is extended.[10] We show in Fig. 12 mainly the potential curves for the resulting E states. It can be seen that the molecule can dissociate from the lowest three MLCT states ($T_{2u}$, $E_u$ and $A_{2u}$, which can mix on extension of an M–CO bond) directly and in an ultrashort time, producing the first excited (1E) state of $M(CO)_5$, in agreement with our observation on excitation in the long-wavelength wing. However, this seems not possible on first sight on starting from the $T_{1u}$ state: the necessary jump from the 2E to the 1E surface near the vertical double arrow has a low probability as a consequence of such a large energy gap. The short time found for the dissociation step on $T_{1u}$ excitation ($\tau_2$ = 18 fs for M = Cr excited at 267–286 nm[13] and about 35 fs for M = Mo in the same range, see Table 1) demands a barrierless continuous path, obviously through a CI instead of a jump between surfaces.

Near the double arrow, the surfaces must be interpreted as a result of an avoided crossing: at large M–CO distance the 1E state has LF character, obviously with $T_{1g}$ parentage, whereas the 2E surface is of MLCT type, correlating with the $T_{2u}$ state. From the avoided crossing one finds the CI by searching within the branching space, which is spanned by the gradient-difference (GD) and nonadiabatic coupling (NAC) vectors.

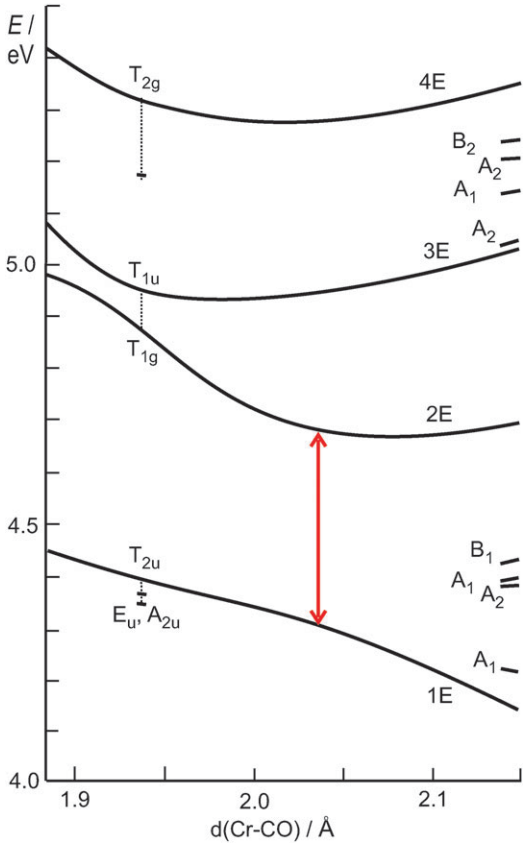


**Fig. 12** Potential curves calculated by a coupled-clusters method with equation of motion[10] for extension of one Cr–CO bond of $Cr(CO)_6$. Note that these distance-dependent potentials resulted from calculations at a lower level than those of Fig. 1. Thus in the latter figure the lowest $T_{1u}$ state of $Cr(CO)_6$ is at 4.3–4.4 eV, with $T_{1g}$ at the same energy, whereas above, $T_{1u}$ is near 4.98 eV in the Franck–Condon region (vertical dotted lines).

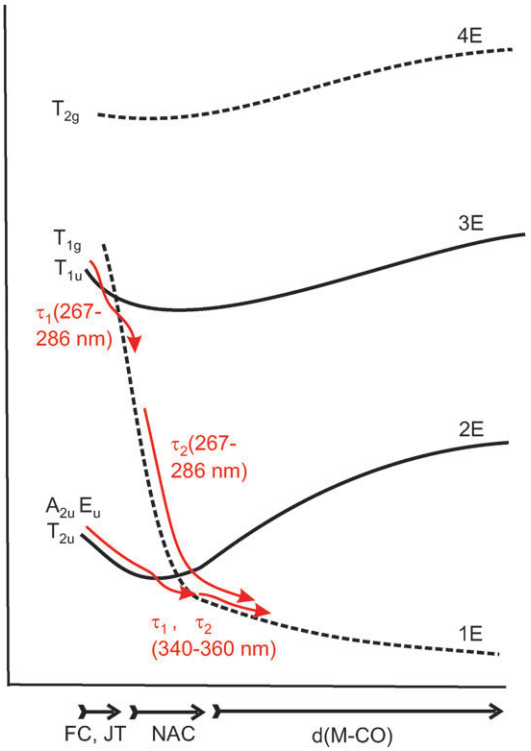


**Fig. 13** Cut through the potential surfaces (shown are only the components correlating with the E states in $C_{4v}$) approximately along the minimum energy paths. The latter is assumed to involve initially Franck–Condon and Jahn–Teller active coordinates (FC, JT), then the nonadiabatic coupling vector (NAC) of the CIs and thereafter stretching of a single MC bond. Potentials with LF character, correlating with $T_{1g}$ or $T_{2g}$, are indicated by broken lines.

The former is the direction of fastest growth of the energy gap; in view of the steep slope from $T_{1g}$ down ultimately to 1E, it is obviously not far from M–CO bond stretching. Hence we have to look for the NAC vector. Both vectors can approximately be calculated at some (not too large) distance from the CI. Symmetry considerations of vibronic interaction (NAC) between two E states (in $C_{4v}$; similarly between a $T_{1g}$ and a $T_{2u}$ state in $O_h$) offer stretching and bending coordinates. The former are probably too close to the GD direction. CMC bending may contribute, however, only with limited activity: it also enables passage of the dissociation product through the $S_1/S_0$ CI; if the slope in this direction were already steep before ejection of the CO, it would induce a premature leakage to the ground state. Therefore we suspect that the NAC vector also involves MCO bending. The assumption of MCO bending before dissociation would explain, why the CO expelled from $W(CO)_6$ has a slightly elevated rotational temperature, as found in photofragment spectroscopy;[30,31] the results agreed well with prediction of an impulsive model, if an initial MCO angle of 170° was assumed.[30] Also the calculations of Paterson *et al.* found a slight bending of an MCO group during dissociation.[17] In Fig. 13, which is a slight modification of our previous Fig. 8c in ref. 13, we summarize these ideas on the early part of the photodissociation. The figure is not a planar cut through the potential surfaces, but a cut close to the minimum-energy paths, so that the direction changes (as indicated at the abscissa) and the cut hits the surface intersections.

From the Franck–Condon (FC) region of any electronic state, the steepest slope (gradient) has components of FC-active and Jahn–Teller (JT) active coordinates. The former have $a_{1g}$ symmetry, corresponding to symmetric MC and CO stretching, which do not lead to dissociation. The latter have $e_g$ and $t_{2g}$ symmetry (pairwise stretching and angle deformation) and are again not dissociative. Thereafter, the wave packet is accelerated in NAC direction. On starting from a higher state, this is necessary to reach the intersection with the LF surface (instead of only the avoided crossing of Fig. 12). But such a direction is also taken on starting from a lower state, because the wave packet does not pass through the CI but goes around the lower cone. Only after arriving at the LF surface, the motion points to M–CO dissociation.

Another interesting detail of the calculation[10] is the prediction that in $Cr(CO)_6$ the $T_{1u}$ and $T_{1g}$ states are practically degenerate (see the ladders in Fig. 1). On first sight, this seems to explain the exceedingly short time (12.5 fs) measured for $T_{1u} \rightarrow T_{1g}$ relaxation on excitation of this carbonyl at 270 nm.[13] (In fact, it is the fastest electron-transfer reaction measured so far.) However, to get distinguishable signals from the two states, the measurement method generally requires

 

**Table 5** Bond dissociation energies (BDE in eV) for three $M(CO)_6$ (from ref. 34)

| | $BDE_1$ | $BDE_2$ | Sum |
|---|---|---|---|
| $Cr(CO)_6$ | 1.48 ± 0.09 | 1.74 ± 0.65 | 3.22 |
| $Mo(CO)_6$ | 1.74 ± 0.09 | 1.52 ± 0.65 | 3.26 |
| $W(CO)_6$ | 2.0 ± 0.09 | 1.74 ± 0.65 | 3.74 |

either a vertical (energetic) or a horizontal (geometric) displacement between them.[32] Therefore the $T_{1g}$ state must be slightly higher than $T_{1u}$ and the slopes from both are steep. In fact, resonance Raman spectra indicate that the $T_{1g}$ level is between the two $T_{1u}$ states.[33] As already argued in ref. 13, the very short progressions in resonance Raman spectra and our short $\tau_1$ indicate that the transition from $T_{1u}$ to the LF surface occurs with very small displacement (as in Fig. 13), although it is not vertical.

In the context of the wavelength dependence, it is helpful to summarize some energies. The pump photons at 270, 286, 303, 341, 350 and 360 nm have energies of 4.6, 4.34, 4.09, 3.64, 3.54 and 3.44 eV, respectively. The probe photon (810 nm) has 1.53 eV. The first and second bond dissociation energies (BDE), determined by photofragment spectroscopy,[34] are compiled in Table 5 for the three $M(CO)_6$. From the same method one can also obtain the energy carried away by the first CO cleaved off from $W(CO)_6$ at 351 nm: it is 0.34 eV on the average, as calculated from the translational, rotational and vibrational temperatures of CO determined in ref. 30. One can see that the two longest wavelengths are not able to cleave off a second CO from $W(CO)_6$, and 350 nm is energetically at the limit for the second step in $Mo(CO)_6$. The vertical $S_0 \rightarrow S_1$ excitation energies of the unsaturated carbonyls $M(CO)_5$ strongly depend on the matrix;[35] but it is assumed that the value for $Cr(CO)_5$ in a neon matrix (1.99 eV) is close to that in the gas phase.[35] In an argon matrix, the excitation of $Mo(CO)_5$ demands an energy that is by 0.59 eV higher than that of the chromium compound;[36] assuming the same difference also for the gas phase, one obtains 2.58 eV for $Mo(CO)_5$. We suppose that $W(CO)_5$ is similar to the molybdenum compound.

### 4.2 Assignment of the oscillations in the parent molecules and the pentacarbonyls

In the Franck–Condon region the oscillations (extracted from the $M(CO)_6^+$ signal, Fig. 2, 3 and 9, see Table 2) should be compared with the vibrational structures observed in absorption in an argon matrix at 10 K.[37] The first allowed (286 nm) band of $Mo(CO)_6$ and $W(CO)_6$ shows a progression of about 350 and 400 $cm^{-1}$, respectively, which was assigned to the totally symmetric ($a_{1g}$) MC stretch vibration;[37] no structure was resolved in the other bands (and with $Cr(CO)_6$). Probably (see Section 3.2 and 3.3), we observed oscillations on pumping in this band and at longer wavelengths (and with $Cr(CO)_6$[13]) with slightly lower wavenumbers (Table 2: 310 and 275 $cm^{-1}$ for $Mo(CO)_6$ and 230 $cm^{-1}$ for $W(CO)_6$). Because their damping time (rate = dephasing rate + population decay) is less than a quarter of the period (~100 fs), the simulation is associated with a large uncertainty. Our values seem hence consistent with the spectroscopic vibrational structures. Generally, a pulse much shorter than a period is expected to coherently superimpose Franck–Condon active vibrational states.

The oscillations with wavenumbers of 80–100 $cm^{-1}$ (Table 2 and, for example, the Fourier transform in Fig. 6) observed in the fragment signals (observation window $L_4$) have already previously been assigned to a pseudorotation oscillation in the ground state of the dissociation product $M(CO)_5$,[11–13] in which the molecule has a square-pyramidal structure ($C_{4v}$); the assignment was confirmed by calculation.[17,18] It involves CMC bending and is illustrated below. There are more such vibrations with similar frequencies (Table 3). But as explained in the next section, only the totally symmetric one ($a_1$, italicized in Table 3) should be expected to be observed with its fundamental frequency.

The saturated hexacarbonyls do not have vibrations of lower frequency. To assign also the oscillation around 35 $cm^{-1}$, we consult the density-functional calculation for $M(CO)_5$ (Table 3). There is only one totally symmetric vibration (86.6 $cm^{-1}$ in $Mo(CO)_5$) in this range; it fits very well with the oscillation at 84 $cm^{-1}$, and there is a similar coincidence for $Cr(CO)_5$. The other vibrations are antisymmetric. The smallest wavenumber corresponds to a $b_2$ type CMC bending (see Fig. 14) with about 50 $cm^{-1}$. We suggest that this vibration causes the 35 $cm^{-1}$ oscillation, however with complications arising from its antisymmetric nature and with some influence of an excited electronic state, both considered in the next section. For convenience, we compare the observed to the calculated frequencies in Table 6.

We also calculated the vibrations in the lowest triplet state (Table 4), in which the molecule has a trigonal-bipyramidal structure ($D_{3h}$). There is no obvious assignment of our two low-frequency vibrations. It is remarkable that the vibrations below 100 $cm^{-1}$ (CMC bending) in this table are all antisymmetric. The next section uses this fact and a symmetry argument, why the observed oscillations should indeed not be associated with a triplet.

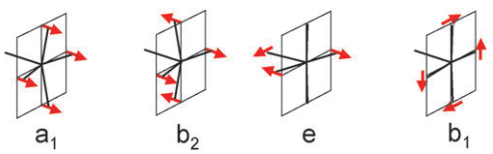


**Fig. 14** Displacement vectors for four CMC bending vibrations discussed in the text.

**Table 6** Observed oscillations *versus* calculated vibrational wavenumbers ($cm^{-1}$) for $M(CO)_5$. The character (CMC bending and MC stretching) and symmetry type in the last line is also taken from the calculation

| | | | |
|---|---|---|---|
| $Cr(CO)_5$ obs.[13] | 352<br>381[38] | 95 | ?[a] |
| $Cr(CO)_5$ calc. | 415 | 96.6 | 49 |
| $Mo(CO)_5$ obs. | 420 | 84 | 36 |
| $Mo(CO)_5$ calc. | 411 | 86.6 | 51 |
| $W(CO)_5$ obs. | | 79 | 32 |
| Character | MC $a_1$ | CMC $a_1$ | CMC $b_2$ |

[a] Uncertain (the shoulder near 40 $cm^{-1}$ in Fig. 6b of ref. 13 was not visible in some data sets).

Fig. 6 shows besides $\nu_a$ = 84 cm$^{-1}$ and $\nu_b$ = 36 cm$^{-1}$ also some peaks with higher wavenumbers. The most prominent one (~165 cm$^{-1}$) seems to be the overtone $2\nu_a$, and two higher members of the progression $n\nu_a$ might also be real. The peak near 123 cm$^{-1}$ suits the combination vibration $\nu_a + \nu_b$. The peak at 420 cm$^{-1}$ can be assigned to a symmetric MC stretch vibration, calculated at 410 cm$^{-1}$ (Table 3). Although weak, it may be real: the corresponding oscillation in $Cr(CO)_5$ (observed at ~352 cm$^{-1}$,[13] calculated at 415 cm$^{-1}$, Table 3) is very pronounced.

To illustrate the vibrations and for later use, we show in Fig. 14 the $a_1$ ($\nu_a$) and $b_2$ ($\nu_b$) displacement vectors (first two diagrams). Obviously their superposition is the pseudorotation coordinate shown at the abscissa of Fig. 11, in which the angle between two ligands decrease from near 180° to 120°; a $D_{3h}$ structure is reached thereby. The other way around, the path down from the $D_{3h}$ conical intersection (along an e′ vector in this symmetry group) can be decomposed into an $a_1$ and a $b_2$ coordinate in $C_{4v}$. By superposition of the first three diagrams one can construct a displacement vector that rotates only one ligand against the rest; after 90°, the ligand is effectively exchanged with the adjacent vacancy. This is the proper pseudorotation coordinate; in Fig. 11 (inset) it leads from one minimum to another *via* a saddle point. The last diagram ($b_1$) together with that for $b_2$ illustrates the two Jahn–Teller active distortion coordinates for E states in $C_{4v}$.

### 4.3 Vibrational selection rules for probe transitions in time-resolved spectroscopy

We consider primarily the cases, in which a resonance plays a dominant role in the probing process. In our experiment, it is a resonance-enhanced multiphoton ionization, in which the long-wavelength probe laser excites the unsaturated carbonyl from $S_0$ to $S_1$ in a region not far from the $S_0/S_1$ CI, from where then additional photons generate the ion (Fig. 15). But one can easily generalize the consideration to cases without resonance, *e.g.* multiphoton ionization or even field ionization, if the distance between the potentials of the involved electronic states varies along a vibrational coordinate and if this distance influences the signal strength (see the example of ethylene below‡).

If the resonance is modulated by a vibration along a coordinate, along which the upper and lower potentials are not parallel, there is a chance to detect it in the form of a coherent oscillation. Since the involved two potentials can be shifted only along totally symmetric coordinates, they are the most important candidates for such phenomena. Those involving a displacement are called Franck–Condon active. Along antisymmetric coordinates the potentials are not shifted, but can have different shapes; the upper and lower potentials belong to the same symmetry group.

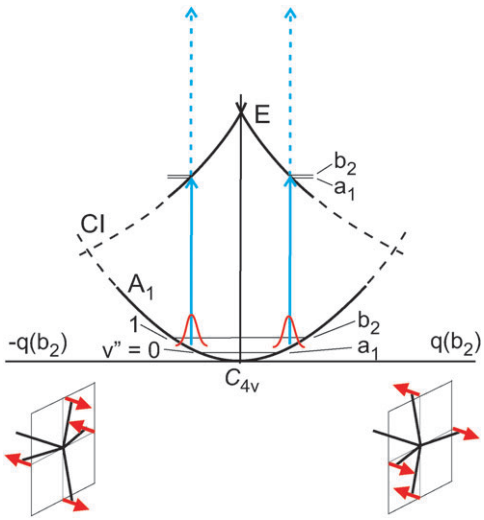


**Fig. 15** Probe transitions with $S_0 \rightarrow S_1$ one-photon resonance far from the $C_{4v}$ equilibrium position in $M(CO)_5$. The upper potential is Jahn–Teller split. The cross section is shown along one of the two ($b_1$ and $b_2$) active coordinates. (Dashed: the path leading to the CI actually also involves displacement along an $a_1$ coordinate.) Displacement along positive and negative $b_2$ direction is illustrated below the abscissa; the two distorted forms are symmetry-equivalent: a 90° rotation around the $C_4$ axis transforms one form to the other. The barrier between the resonant locations in the upper potential is assumed high (although lower than the cusp: the saddle point is displaced from the cusp in $b_1$ direction, the second JT-active coordinate), so that the vibrational levels are grouped in pairs with small energy distance, resulting from tunneling splitting. Note also that the states with even or odd quantum numbers are totally symmetric ($a_1$) or have the symmetry of the coordinate ($b_2$), respectively.

It is another general property of antisymmetric coordinates that locations of positive and negative departure are symmetry-equivalent. This is illustrated in Fig. 15, which shows below the abscissa the structures of a $C_{4v}$ pentacarbonyl with positive and negative $b_2$ distortions: the sign just interchanges the roles of the two pairs of equatorial ligands, and the two forms can be interconverted by a 90° rotation around the $C_4$ axis.

The figure also shows a wave packet (which can be understood as a superposition of two or several vibrational wave functions, *e.g.*, with $v'' = 0$ and 1) at the two turning points. With the probe wavelength in resonance just there (as shown), one expects a signal maximum at both turning points, *i.e.*, twice per vibrational period. Hence an antisymmetric vibration should only give rise to overtones. On the other hand, according to the preceding section a fundamental of the $b_2$ vibration has been observed in $Mo(CO)_5$ and $W(CO)_5$ (Section 4.2). (For further such observations, see below.) This is surprising and not intuitive in a picture such as Fig. 15. For understanding the phenomenon we have to consider the transition amplitudes instead of the probabilities alone.

‡ A referee pointed out that for derivation of vibrational selection rules the assumption of an intermediate resonance is not necessary for $M(CO)_5$: direct multiphoton ionization would lead to the ion ground state, which has the same symmetry as $S_1$ of the neutral; it is also subjected to Jahn–Teller (JT) distortion with the same JT-active coordinates ($b_1$ and $b_2$). The considerations in this section would then lead to the same selection rules, if JT splitting is large and tunneling splitting small. We prefer the description with the resonance enhancement, (1) because a one-photon absorption may be more familiar to many readers and (2) because the resonance seems to us to be established by the spectroscopic data for $Cr(CO)_5$ and $Mo(CO)_5$ (end of Section 4.1) and its strong enhancement is supported by the wavelength dependence of ionization and fragmentation.[39] The resonance also allows a rationalization, why the signal is modulated by the $b_2$ mode (due to the slope from the CI) and not by $b_1$ (which is also JT active) and the differences between the different carbonyls (Section 4.4), even its absence in $Fe(CO)_4$.[14]

 

We keep the following derivation brief and use simple examples, because a more detailed analysis, based on linear response, is available[40] which, however, considered only totally symmetric vibrations.

Suppose that at time zero we have a 1 : 1 superposition ($\psi''$) of vibrational states $v''$ and $v''+1$ (symmetries a and b) which is then probed at the time $t = t_{pr}$:

$$\psi'' = \varphi''_a \exp\left(i\frac{E''_a}{\hbar}t_{pr}\right) + \varphi''_b \exp\left(i\frac{E''_b}{\hbar}t_{pr}\right) \qquad (2)$$

$\varphi''_a$ and $\varphi''_b$ are the stationary (spatial) wave functions with the energies $E''_a$ and $E''_b$. In the exponents, arbitrary phases $i\varphi''_a$ and $i\varphi''_b$ have been omitted. The one-photon resonant probe process will populate the vibrational states

$$\psi'_a = \varphi'_a \exp\left(i\frac{E'_a}{\hbar}t\right)$$
$$\psi'_b = \varphi'_b \exp\left(i\frac{E'_b}{\hbar}t\right) \qquad (3)$$

and perhaps more such states on the higher electronic surface. Phases have again been left out. The probe laser creates two polarization amplitudes (oscillating between the lower and upper electronic states), containing the scalar products $\langle\psi''|\psi'_a\rangle$ and $\langle\psi''|\psi'_b\rangle$. These amplitudes must be added. Omitting for the moment a common factor $F_{pr}\mu$, the product of the (time-dependent) electric field amplitude of the probe with the electronic transition moment, we can write:

$$\langle\psi''|\psi'_a\rangle + \langle\psi''|\psi'_b\rangle = \langle\varphi''_a|\varphi'_a\rangle \exp\left(-i\frac{E''_a}{\hbar}t_{pr} + i\frac{E'_a}{\hbar}t\right) + \langle\varphi''_b|\varphi'_b\rangle \exp\left(-i\frac{E''_b}{\hbar}t_{pr} + i\frac{E'_b}{\hbar}t\right) \qquad (4)$$

(Note that scalar products between a and b terms vanish because of symmetry.) The magnitude squared of it is the corresponding (oscillating) probability of finding the system on the $v'$ level of the upper electronic state; these squares can be considered time-dependent Franck–Condon factors. Defining $\Delta E'' = E''_b - E''_a$ and $\Delta E' = E'_b - E'_a$, one finds

$$|\langle\psi''|\psi'_a\rangle + \langle\psi''|\psi'_b\rangle|^2 = \langle\varphi''_a|\varphi'_a\rangle^2 + \langle\varphi''_a|\varphi'_a\rangle\langle\varphi''_b|\varphi'_b\rangle \times \exp\left(-i\frac{\Delta E''}{\hbar}t_{pr} + i\frac{\Delta E'}{\hbar}t\right) + \langle\varphi''_a|\varphi'_a\rangle\langle\varphi''_b|\varphi'_b\rangle \times \exp\left(+i\frac{\Delta E''}{\hbar}t_{pr} - i\frac{\Delta E'}{\hbar}t\right) + \langle\varphi''_b|\varphi'_b\rangle^2 \qquad (5)$$

To calculate the population and the signal, we have to multiply this expression by the square of $F_{pr}\mu$, the factor omitted above, or alternatively by a cross section and the probe intensity (or a suitable power of it in the case of a multiphoton transition); then one must integrate over $t$, because the detection takes place only after the end of the probe pulse. The latter can be a Gaussian centered at $t = t_{pr}$. The more interesting case is, if the probe pulse is much shorter than a vibrational period. (If not, this vibration is not resolved in the signal.) Ideally, we can replace it by a $\delta$ function centered at $t = t_{pr}$; then on integrating (5) for calculating the oscillating part of the signal ($S_{osc}$), we can replace $t$ by $t_{pr}$. Substituting $\nu'' = \Delta E''/h$ and $\nu' = \Delta E'/h$ and contracting the exponentials in (5) to a cosine, we find for the oscillatory part of the signal

$$S_{osc} \propto \cos(2\pi(\nu'' - \nu')t_{pr}) \qquad (6)$$

If the vibrational frequencies in the upper and lower electronic states, $\nu'$ and $\nu''$, differ only little, the period of (6) is too long to be detected. That is, the fundamental of an antisymmetric vibration is then in fact not seen as an oscillation. If, however, $\nu'$ is near zero, such as in Fig. 15 where it is the result of a tunneling splitting, then $\nu'' - \nu' \approx \nu''$, which appears as the fundamental in the detection. If the tunneling splitting is larger and hence $\nu'$ does not vanish, the observed oscillation frequency $\nu'' - \nu'$ will be smaller than the ground-state frequency. This perhaps applies to our case, where the calculated wavenumber $\nu''/c$ is 51 $cm^{-1}$ as compared to the observed one of 36 $cm^{-1}$ (Tables 2 and 3).

The frequency difference $\nu'' - \nu'$ is also observed in the vibrational structure of the frequency-domain spectrum of an electronic transition. In fact, the simple expression (6) can be understood as the cosine Fourier transform of such a spectrum with just two vibrational lines. We suppose that this result can be generalized for the case of more than two vibrational levels, more than one vibration including also totally symmetric ones and with consideration of different relative intensities: the oscillating part of the probe-delay ($t_{pr}$) dependence will just be the Fourier transform of the spectral structure in the electronic transition that is resonant with the probe laser. This implies that *the vibrational selection rules for time-resolved and frequency-domain spectroscopies will be the same*.

The more detailed analysis of ref. 40, based on linear response, considered only totally symmetric vibrations, as mentioned. However, it also uses the Fourier transformation for conversion from time to frequency domain. Therefore this work would imply the same selection rules.

In frequency-resolved spectroscopy, $\Delta v \neq 0$ can be observed in electronically allowed transitions, if the vibration is totally symmetric and the upper and lower potentials are displaced against each other;[41] their relative intensities are controlled by the Franck–Condon factors, which depend on the displacement of the potentials. Antisymmetric vibrations are in general observed only as overtones and only if the potentials differ in shape (they are not displaced in such a direction).[41] Fundamentals of them can be observed, if the upper vibrational levels occur in pairs with negligible energy difference, which typically results from tunneling splitting if the barrier is high;[41] such a situation arises, if the upper state has a maximum (or a cusp as in Fig. 15) vertically above the ground-state minimum, and if the observed transitions lead to levels far from the maximum and far from the equilibrium geometry. An example is the torsion vibration (antisymmetric, $a_u$ in $D_{2h}$) of ethylene, whose fundamental is observed in the long-wavelength wing of the UV absorption spectrum; these transitions lead to levels with non-resolved tunneling splitting near the excited-state

minimum, in which the molecule is twisted by 90°.[41] These same fundamentals were recently also observed in time-resolved spectroscopy of ethylene;[42] in this case the detection was by multiphoton ionization (lower state of the transition: $S_1$ of ethylene with its 90° twist; upper state: ion ground state with a cusp at this geometry) as in this work, but probably without any intermediate resonance. In fact, one can use the generalized Franck–Condon factors (5) or (6) also for a multiphoton transition such as from the neutral molecule to the ion. A similar case was the torsion vibration in the ππ* minimum of $C_2F_4$ observed by the same technique in ref. 43 but interpreted there as an overtone instead of a fundamental. Similarly, excited hexafluorobenzene showed a nonplanar ($e_{2u}$) vibration, according to the calculations probably its fundamental;[44] in this case, the negligible tunneling splitting would be in the lower level of the probe transition (involving again multiphoton ionization). Other cases of antisymmetric vibrations observed in time-resolved spectroscopy involved only overtones of wagging and torsion types in planar derivatives of 4-aminobenzonitrile, whereas fundamentals were also observed in derivatives with sufficient perturbation of planarity (survey in ref. 45). Coherent oscillations in the ground state have been observed after photochemical *cis–trans* isomerization of rhodopsin, which have been assigned to C=C torsion;[46] it was not discussed, whether the observed frequency corresponds to an overtone or the fundamental. In $S_1$ of azulene, two low-frequency oscillations were observed by the transient $S_0 \rightarrow S_1$ excitation,[47,48] which were tentatively assigned to out-of-plane (hence antisymmetric) vibrations,[47] probably not in the Franck–Condon region.[48]

For convenience, Fig. 16 summarizes the selection rules, which oscillations to expect from totally symmetric (A) and antisymmetric (B to D) vibrations, if the electronic transition is allowed. Only a ↔ a and b ↔ b transitions are allowed. In the cases A and B with similar level distances in the lower and upper states, the difference $\nu'' - \nu'$ is small, so that it will normally not be observed as an oscillation in time-resolved spectroscopy. The situation with very small $\nu'$ arises typically from tunneling splitting, which is small if a large barrier separates two minima. In this case, the fundamental $\nu''$ of the antisymmetric vibration is observable, both, with time and frequency resolution. D shows a case (*e.g.* ethylene) with tunneling splitting in both, the lower and upper states. Here we should mention that there may also be tunneling splitting in $S_0$ of $M(CO)_5$, because there are multiple minima. As case D in Fig. 16 shows, the selection rules will not be affected thereby. We also do not expect complications for these rules by the fact that there are three (or six, if the other CI is taken into account) minima instead of only two; in this case, the splitting (also in $S_1$) must be analysed in the higher symmetry group $D_{3h}$ ($O_h$), and degenerate levels can arise. In the figure, we have assumed that before the probing there is a coherence (prepared by the pump process, for instance) only in the lower state. In this case, any superposition of upper vibrational levels prepared by the probe from a common lower level will not appear as a $\nu'$ oscillation because of the time-integration over the probe pulse. The situation may be different, if the probe and pump transitions are the same (one-wavelength experiment), so that coherences may exist in both states before probing.

Although this is the result of the mathematics above, it is not yet intuitive in the time-resolved case: why should the signal from the left and right turning points in Fig. 15 not be the same, so that two maxima per vibrational period (hence only an overtone) should be observed? Or: how is the symmetry of Fig. 15 broken? For an answer, we suggest to

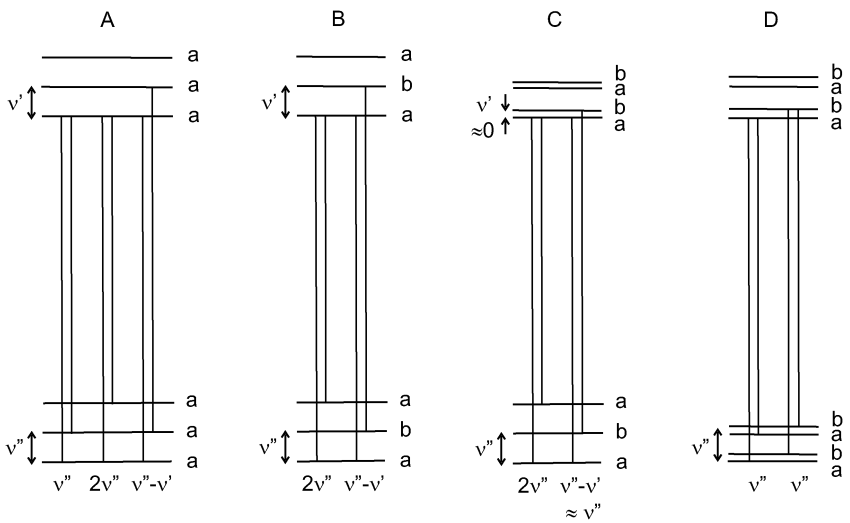


**Fig. 16** Vibrational selection rules, if the probe transition is electronically allowed. (A) With totally symmetric vibrations (a type), the fundamental and overtones can be observed, with intensities governed by the Franck–Condon factors. The difference frequency $\nu'' - \nu'$ will in general be too small (the period too long) to be identified in time-resolved spectroscopy. (B) With an antisymmetric vibration (b type), only overtones can be observed, unless (C) the difference frequency $\nu'' - \nu' \approx \nu''$, because each of the upper levels is double due to tunneling splitting. D shows the case where both sets of vibrational levels are double, with negligible a–b splitting. In (A–D), the transitions from a common lower level to different upper levels have been omitted; they are only observable in frequency-domain spectroscopy. In the time domain, they are not expected, because the probe-delay dependence reflects only processes occurring before probing.

 

reconsider the expressions above. Thus the function (4) can be understood as the scalar product $\langle\psi'|\psi''\rangle$ of $\psi''$ with

$$\psi' = \psi'_a + \psi'_b \qquad (7)$$

which are functions of $t$. Later, the squared magnitude of (4) (*i.e.*, (5)) is multiplied with $\delta(t - t_{pr})$ (an ideally short probe pulse) and integrated over $t$, a procedure which only replaces $t$ by $t_{pr}$ in (5). If this substitution is already done in (4) or (7), the end result is the same. In this interpretation, the probe pulse generates from the lower coherent superposition $\psi''$ another superposition $\psi'$ in the excited state, or projects $\psi''$ onto $\psi'$. It is important to note that this projection is phase-locked: if at one $t_{pr}$ there is a plus sign in (7), it will be plus also at another probe delay, because it is inherited from $\psi''$, where it is fixed before probing. (Another phase would, for example, involve a minus sign in (7), or generally a factor $\exp(i(\phi''_b - \phi'_b))$ before $\psi_b$. Which phase is valid for a given case, must be found out by separate considerations.) The sum in (7) has a spatial part which is localized *e.g.* on the right-hand side in Fig. 17; its time-dependent part transforms it to the left only very slowly, in a time $1/2\nu'$. Hence, before this time, the scalar product $\langle\psi''|\psi'\rangle$ and its squared magnitude (the Franck–Condon factor) will not vanish on the right-hand side but will be zero on the left. That is, the symmetry-breaking of Fig. 15 and 17 can be made plausible by consideration of the phases and their locking: *the phase in superposition of $\psi''_a$ with $\psi''_b$ is established by the way of its preparation (in the pump process); it is conserved ("locked") when it is projected to the superposition of $\psi'_a$ with $\psi'_b$ by the probe, at any time of its variable delay*, as long as this delay is short compared to the tunneling time in the upper state.

### 4.4 Implications for the potential of $M(CO)_5$, $M(CO)_6$ and the reaction path

As we previously suggested, the oscillation of a wave packet is stimulated by acceleration on the slope of the potential. (This view can even be maintained in the Franck–Condon region; conventionally, the phenomenon is described there by the superposition of Franck–Condon active vibrations.) If the vibrational coordinate can be assigned, one can identify the direction of the slope. As explained in Section 4.1 (see also ref. 11–13), the wave packet arriving after dissociation at $S_1$ of

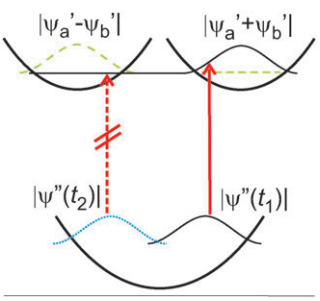


**Fig. 17** A wave packet $\psi''$ oscillating in a single-minimum potential (bottom), shown at two different probe times $t_1$ and $t_2$, and (top:) a wave packet in a double-minimum potential. The latter stays localized *e.g.* on the right-hand side (because it involves the same phase as in the $\psi''$ superposition) over times short compared to the tunneling time, so that the transition probability at time $t_2$ vanishes.

$M(CO)_5$ passes through a conical intersection (CI). At the CI the molecule has a trigonal-bipyramidal geometry and the electronic state is degenerate by symmetry (E′ in $D_{3h}$). Jahn–Teller (JT) splitting along the JT active e′ coordinates (which open a 120° angle between two ligands of the equatorial plane) connects it just with $S_1$ (*i.e.* one of its degenerate components) and $S_0$ at square-pyramidal ($C_{4v}$) geometry. The e′ direction decomposes in $C_{4v}$ into a sum of an $a_1$ and $b_2$ bending displacement vectors (Fig. 14). Therefore the observation of the $a_1$ and $b_2$ vibrations fully supports the ideas on the path through such a JT-induced CI down along a JT-active coordinate.

We also suggested[12] that the probing is only sensitive to the radial component (Fig. 11; e′ in $D_{3h}$, $a_1 + b_2$ in $C_{4v}$), not to any circular component, because only along the slope from the CI the $S_1$–$S_0$ distance is tuned over a resonance with the long probe wavelength (Section 4.1). Furthermore, we assumed that the resonance is met only in the direction to the $C_{4v}$ minima, not towards the saddle points, because there the $S_1$–$S_0$ gap is too small (inset in Fig. 11). In this way we explained, why with short pump wavelengths the oscillation appears only with delay (see the first maximum in Fig. 7), suggesting that the wave packet first arrives at a saddle point (inset in Fig. 11). This detail was confirmed by calculation.[17,18] The wavelength dependence of this delay (Fig. 7) and of $\tau_3$ (Table 1) now provides us a refinement: from the latter dependence in $Cr(CO)_6$ we concluded[13] that at longer wavelength the wave packet takes a lower-energy path on the LF surface, so that it arrives earlier at the $S_1/S_0$ CI of $M(CO)_5$, as outlined in Fig. 11. The $\tau_3$ dependence (although only determined at a few wavelengths) in Table 1 suggests to extend this conclusion also to the two heavier carbonyls. In addition, from Fig. 7 we conclude that not only the energy of entrance to the $S_1$ surface changes but also the direction: whereas $\tau_3$ at 340–360 nm is shorter by about 15 fs than at 286 nm (Table 1), the first prominent maximum appears earlier by ~100 fs or even 500 fs (*i.e.*, one period in addition). That is, in this case the wave packet enters to $S_0$ directly into a minimum. The path before leads it through a valley (actually one of three) on the $S_1$ surface to the CI, and this valley is obviously above an $S_0$ saddle point. This is shown in the inset of Fig. 11, where the dotted arrows indicate the path at long pump wavelengths, whereas the solid ones apply for excitation of the $T_{1u}$ state (286 nm), for example. (Note that, to match this finding, the funnel has now been rotated by 60° compared to the previously suggested potential.[12,13]) According to this figure, at short wavelengths the wave packet does not reach one of the $S_1$ valleys in the short time before arriving at the CI but moves still near a ridge (or a cusp). (The drawing is based on a simple mathematical function and does not show a cusp, which would result from Jahn–Teller splitting of the E state. It also does not reflect the fact that each minimum has two CIs in its neighborhood. A better figure is difficult to draw, because more than two coordinates are involved.)

A question is, whether the observed oscillations take place in a single of the three $S_0$ wells or whether they are delocalized, passing over the barriers between them. Whereas the DFT calculations (Section 3.4) assumed the former (with harmonic approximation), the wave packet dynamics of ref. 18 suggested

the latter. The corresponding wave function must then be classified in $D_{3h}$ and probably belongs to the e′ species. In this case the lower frequency will again be an apparent fundamental (actually $\nu'' - \nu'$), if $\nu'$ is again very small and results from tunneling splitting. The 84 $cm^{-1}$ oscillation must then be assigned to an overtone of it; a totally symmetric bending vibration does not exist in this symmetry group. The question could be decided by analysis of overtone and combination vibrations, which would require a further improvement of the signal-to-noise ratio. However, we prefer an assignment to vibrations in one of the wells, in particular, because the calculated $a_1$ bending frequencies for both, $Mo(CO)_5$ and $Cr(CO)_5$, fit well to the observed oscillations (Table 6).

A photochemical argument also supports this assignment: In solution after photoelimination of a CO group in *trans* position to a ligand L in a substituted carbonyl $LM(CO)_5$, a new ligand L′ enters specifically in *cis* position (product: *cis*-$LL'M(CO)_4$, see textbooks[2,49] or the discussions in ref. 12 and 50). This has been a puzzle for a long time[12,50] but can be easily explained by the single-step pseudorotation (single exchange of a vacancy with an adjacent CO) on $S_1 \rightarrow S_0$ relaxation through the CI in the primary dissociation product $LM(CO)_4$.[12] By contrast, the delocalized vibration would imply multiple exchanges of vacancies and ligands, so that statistical mixtures of *cis*- and *trans*-$LL'M(CO)_4$ would be expected. This conclusion is valid, if this low-frequency vibration lives long enough in solution and is not deactivated in less than one period ($\sim$1 ps for the $b_2$ fundamental and $\sim$350 fs for its overtone or the $a_1$ fundamental; typical vibrational deactivation times in solution are 10–15 ps, see *e.g.* ref. 51 and 52).

It seems thus more probable that the observed oscillation takes place only near the minimum of a well and does not overcome the saddle points. Hence only a small fraction of the available energy appears in the vibration that is observed.

The photochemical *cis* effect supports another detail of our mechanism: on arriving at $S_0$, the wave packet does not explore the full surface but reaches only two of the three minima of the inset of Fig. 11 (four of the six available minima, if the other CI is also considered). These minima are just those, in which the original ligand vacancy is swapped with an adjacent (*cis*) CO group, whereas the minima corresponding to the original orientation of the vacancy or to its (pseudo-) rotation by 180° (*trans* orientation) are not reached. (This has previously not been recognized, *e.g.* in the recent review.[19] Equal probability of all vacancy orientations was also assumed to explain the limited yield of recombination of CO with $M(CO)_5$ in condensed phase;[35,36] but indeed this yield varies.[36] On the other hand, the reorientation of the vacancy is certainly a good rationalization, why recombination is not quantitative even in a stiff matrix.) Hence the wave packet does not move in a diffusive way but is guided by slopes and the accumulated momentum; its path does not fill the phase space but is more or less one-dimensional (except some branchings), although some excess energy is steadily fed into other degrees of freedom. It is interesting that such fine details have photochemical consequences. Dissociation combined with isomerization is also observed in more complicated complexes with sixfold coordination such as the Ru complexes investigated in ref. 53 (more examples are quoted in ref. 54). We suggest that this phenomenon is characteristic for a process passing through the $S_1$ state of the dissociation product, which then relaxes through the CI to $S_0$ with a single-step pseudorotation.

In the preceding section, we ascribed the apparent observation of the $b_2$ fundamental to a situation, in which the corresponding vibrational frequency in $S_1$ is very small, such as in tunneling splitting. This implies that the cusp in $S_1$ is high and that JT splitting in $S_1$ is energetically efficient in this $b_2$ direction (Fig. 15). We can infer two things:

(1) The observability of the fundamental depends on the tunneling splitting at the energy reached by the probe laser, hence also on the $S_1$ energy. The latter is different in the pentacarbonyls of Cr, Mo and W (see the energetics at the end of Section 4.1). Therefore it is not surprising, why the fundamental was clearest in the Mo case, less distinct in $W(CO)_5$ and very uncertain with $Cr(CO)_5$. Another observation can also be understood by a resonance: Fig. 8 shows intensity ratios of the 36 $cm^{-1}$ over 84 $cm^{-1}$ oscillations that favor the antisymmetric vibration in the $Mo(CO)_5^+$ signal but the symmetric one in the $Mo(CO)_4^+$ signal. This is natural, if the parent ion ($Mo(CO)_5^+$) has a resonance along the same coordinate as the neutral but without the small tunneling splitting in the upper state, so that instead of Fig. 16B and C will apply, in addition to Fig. 16A. In this case only the symmetric ($a_1$) vibration enhances the ionic absorption and thus fragmentation and production of $Mo(CO)_4^+$; motion along the $b_2$ coordinate in the neutral will then only enhance the corresponding overtone in this ion signal.

(2) The efficient JT splitting implies that the CI ($D_{3h}$) is clearly below the cusp of $S_1$ (E state, $C_{4v}$). In fact, we already noticed in dissociation of $Cr(CO)_6$ that even the longest wavelengths produced the $S_1$ state of $Cr(CO)_5$, although the energy was not sufficient to reach the cusp of $S_1$,[13] and we concluded that the path at long wavelengths reaches the funnel just a little above the CI; that is not far from trigonal bipyramidal ($D_{3h}$) geometry, or probably above the $S_0$ saddle region (see above) with one ligand half-way to the exchange with the adjacent vacancy (symmetry $C_{2v}$). Now we can extend this statement to the Mo and W case: also here the oscillations are the same (except minor differences in the phases) for all pump wavelengths and the kinetic scheme shows only slight differences in the time constants and the appearance time of the oscillations. In view of the efficient JT splitting of the E state, we can suppose that the JT activity already begins much earlier on the E surface (resulting from the dissociative $T_{1g}$ ligand-field state on extension of a metal–ligand bond), soon after it is reached. In fact, this was predicted by Paterson *et al.*[17] Hence there is an early acceleration of the wave packet to the CI seam leading to $S_0$. It is therefore amazing that the molecule is still in an excited state after dissociation. Perhaps the dissociation times ($\tau_2 \approx 20$ fs for M = Cr[13] and 30–35 fs for M = Mo and W) are just too short for a bending motion ($\tau_3$ = 42–55 fs) to be completed, in spite of the early beginning.

In the context of the resonance enhancement (point 1 above), we may also add a conclusion on the ionization mechanism by the probe laser: we use intensities near $10^{13}$ W $cm^{-2}$ at 800 nm. Because this corresponds to an electric-field amplitude

 

of 1 V $Å^{-1}$, it is usually believed that this field causes the ionization (optical or intense field ionization) and that this field also shifts molecular levels and distorts potentials. In this picture there is no place for a resonance (see, *e.g.* ref. 55). However, in pure field ionization there is probably no chance to understand the pseudorotation oscillations and in particular the observed $b_2$ antisymmetric fundamental (and its absence in $Cr(CO)_5$) without the properties of the $S_0$ and $S_1$ potentials with a maximum (cusp) of the latter (causing tunneling splitting) above the minimum of the former. A key difference of the examples with very large transition moments considered in ref. 55 from our case may be that the $S_0 \rightarrow S_1$ bands in $M(CO)_5$ are weak, because they involve a d $\rightarrow$ d transition. (The transition moment couples with the field and in first order causes the shifts.[55]) Already previously we pointed to the importance of resonances in high-intensity dissociative ionization of carbonyls[39] and other systems,[32] as also did the group of Nakashima and Yatsuhashi *et al.* (*e.g.* ref. 56 and 57).

### 4.5 Triplets?

The vibrations and the relaxation path have been discussed above with potentials belonging to the singlet manifold. The oscillations (around the $C_{4v}$ minima) are excited by acceleration of the wave packet on the slope on leaving a JT-induced CI ($D_{3h}$ symmetry). By contrast, the lowest triplet ($^3A'_2$) of $M(CO)_5$ has its minimum at $D_{3h}$ symmetry, as confirmed by our DFT calculation and in ref. 27. All low-frequency vibrations are antisymmetric (degenerate) in this state (Table 4). If the observed two oscillations should be assigned to them, one would have to assume that two antisymmetric fundamentals were observed. That is, one had to postulate a resonant excited state with tunneling splitting along two coordinates. Such a state is not known. Even if one considers the alternative assignment of the 36 $cm^{-1}$ as a fundamental and the 84 $cm^{-1}$ as its overtone, there are many details which are easily explained in the singlet model but seem difficult to understand with a triplet assumption. In particular, with the triplet there is no analog of the CI and its slope that would stimulate the oscillations as in the singlet manifold. We conclude that there is no triplet contribution to the observed oscillations and relaxation path. It is interesting that this statement (which was already emphasized previously[12,13] for 270 nm excitation) is also valid (a) in the long wavelength wing of the absorption spectrum and (b) with the heaviest metal (W).

The absence of a triplet contribution is in contrast to the suggestion of textbooks[2,49] and of some—also recent[9]—quantum chemical calculations that singlet–triplet transitions contribute to the long-wavelength absorption wing in particular in the heavier $M(CO)_6$. It seems also to contradict the phosphorescence observed from many substituted $d^6$-metal complexes under cryogenic conditions (reviewed in ref. 58). However, our mechanism involves a relaxation from the initially excited (singlet) MLCT state *via* an avoided crossing to the repulsive LF state. The avoided crossing may imply a barrier; in the three metal hexacarbonyls, it is certainly small, even from the lowest excited state, as to judge from the short $\tau_1$. But for cryogenic temperatures, it may be sufficient to cause a lifetime that is long enough to allow for some fluorescence, as observed at 10 K in ref. 59 for the three $M(CO)_6$. With a higher barrier, the lifetime at low temperature will even be longer, which may suffice to allow for some intersystem crossing.

We suggested a higher barrier, resulting from a larger LF-MLCT gap, in $Ni(CO)_4$[15] and $Re_2(CO)_{10}$[16] to explain the longer dissociation times. A much higher barrier can be expected in complexes, where the MLCT state is lowered compared to the LF state, *e.g.* in negatively charged isoelectronic systems such as $Nb(CO)_6^-$ or $Ta(CO)_6^-$,[60] or if some ligands with low-lying $\pi^*$ orbitals (*e.g.* dipyridyl or other diimines; see the review of Vlček[61]) or with stronger donor properties (such as amines) substitute some CO groups (many of the examples reported in the review of Lees[58]). The triplet emissions in them can be interpreted by the avoided-crossing model with sufficiently high barrier and long enough lifetime to enable intersystem crossing. Unusually long times for the elimination of CO from mixed Ru complexes[54] and from $(C_6H_6)M(CO)_3$, M = Cr or Mo,[62] were also interpreted by barriers resulting from avoided crossings, although only between charge-transfer states.

The model can probably also rationalize wavelength dependent photochemistry in examples such as those reviewed in ref. 63: whereas at short wavelength a CO is cleaved off in ultrashort time within the singlet manifold, so that the unsaturated complex can be active in CH activation, at long wavelength (below the dissociation barrier) the lifetime is long enough, so that intersystem crossing takes place in the intact molecule; the excited triplet then shows different reactions (*e.g.* metal–metal bond splitting in dinuclear carbonyls) or phosphoresces. This rationalization of the wavelength dependence (anti-Kasha behavior) is also in agreement with another feature of our mechanism: from a higher MLCT state, the molecule does not relax vertically to a lower state (where it would again be delayed by the barrier, so that transition to the triplet manifold might occur) but downhill with large horizontal components; it is geometrically distorted, driven by slopes on the potential, and then passes by a CI directly to the repulsive surface. Although the same surface can also be reached from lower states (Fig. 11), other channels (fluorescence or intersystem crossing) may be competitive from them, if their lifetime is long enough.

### 4.6 Intramolecular vibrational relaxation?

Fig. 11 or 13 indicates the path of the wave packet down along the slopes of potential energy surfaces. In this way, electronic energy is converted to kinetic energy of the nuclei. If the path was along a straight one-dimensional coordinate, this simple picture suggests that the energy remains just in this degree of freedom. In fact, the path repeatedly changes direction (Fig. 13). If the turn of the valley is sudden, kinetic energy remains in the preceding coordinate, causing vibrations along it. In this way, vibrational energy can accumulate in a limited number of degrees of freedom, without any intramolecular vibrational redistribution. However, there must also be some diffusion of energy out from the drawing plane of, *e.g.*, Fig. 13. This can be inferred from the observation (Section 4.4) that

only little energy is contained in the coherent oscillations, too little to climb over the saddle points, for example, perhaps very few quanta of a 36 $cm^{-1}$ and a 84 $cm^{-1}$ vibration (Section 4.4). This is a very small fraction of the total available energy (around 2.25 eV or 18 000 $cm^{-1}$ with 270 nm excitation; *i.e.*, the energy of the photon (4.6 eV) minus that of dissociation (2.0 eV) and that carried away by CO (0.34 eV) according to data of ref. 30 for $W(CO)_6$) (see end of Section 4.1). Previously, we made a similar and more quantitative observation in dimethylaminobenzonitrile.[64]

It is popular to assume that the energy is dissipated from the active modes (the coordinates of the drawing plane in Fig. 13) to other degrees of freedom ("the bath") by means of a system–bath interaction ($H_{sb}$), which is called Redfield model. Calculations use the reduced-density matrix method; see, for example, the application to charge-transfer reactions in ref. 65 and to a case (pyrazine) with conical intersection and coherent oscillations in ref. 66 and 67. Such a relaxation is expected to be exponential in time and tend towards equipartition. Both are not consistent with our observations:

(1) The relaxation from the $S_1/S_0$ CI to an $S_0$ minimum in $Mo(CO)_5$ takes less than 56 fs ($\tau_3$). This process converts electronic to vibrational (or nuclear kinetic) energy (E → V relaxation). During this time most energy is dissipated to other degrees of freedom and only little is conserved in the pseudorotation coordinates; that it is only little in this degree of freedom is inferred from a photochemical argument and the assignment of the coherent oscillations (Section 4.4). The latter then takes 1–1.5 ps ($\tau_{deph}$) to decay. Obviously the lifetime of energy in the pseudorotation mode cannot be characterized by a constant $H_{sb}$, *i.e.*, by the same time constant as for the preceding E → V relaxation. It is suggestive to assume instead that the redistribution rate depends on the location on the potential surface and is particularly fast, where the surface is most anharmonic, such as near a CI.

(2) As pointed out above (Section 4.4), the system reaches only four of the six symmetry-equivalent $C_{4v}$ minima of $M(CO)_5$, which could be interconverted by pseudorotation and would statistically be equally probable. This assumption is necessary to explain the nearly exclusive formation of *cis* products from substituted carbonyls. It was readily explained by the wave packet motion, which is not diffusive but driven by slopes and accumulated momentum.

It was already noticed for the chromium carbonyl in ref. 13 that, compared to prediction by equipartition, the elimination of a second CO group from the "hot" $S_0$ (time constant $\tau_4$) is too fast and also depends less than expected on the excess energy, *i.e.*, on the pump wavelength. For example (see the energies at the end of Section 4.1), with the sum of the two first dissociation energies for $Mo(CO)_6$ (3.26 eV, Table 5) and the assumption that the first CO carries 0.34 eV away as with the tungsten system, with the pump wavelength of 341 nm (3.64 eV) there is only 0.06 eV of excess energy for cleaving off the second CO. With 350 nm (3.54 eV), there is even no excess energy at all. Nevertheless, this ground-state dissociation is very fast ($\tau_4 \approx 3$ ps, Table 1) in both cases. For the longer wavelength, it must probably be assumed (a) that only those $Mo(CO)_5$ dissociate, for which the first CO elimination has left enough energy, more than the average value (a rather small pedestal of the $Mo(CO)_5^+$ signals at long delays can be interpreted in this way) and (b) that the dissociation energies are actually a bit smaller than in Table 5 (error limit ≈ 0.6 eV). But even then the dissociation is much faster than expected with statistical distribution of the energy. Obviously the MC stretch modes contain more energy than expected from equipartition.

## 5. Concluding remarks

Although according to Section 4.3 the vibrational selection rules are the same for time-resolved spectroscopy as in electronic transitions in frequency-domain spectra, it should be emphasized that in the time domain the case of an antisymmetric fundamental is very nonintuitive. Let us take an example that may be more common than the unsaturated carbonyls: if in ethylene there is a wave packet oscillating in torsional direction ($a_u$ in $D_{2h}$), why should the signal be different for positive and negative torsion angle? If the signals are the same, one should observe (at least) two signal maxima per period, be they at the turning points (which are symmetry-equivalent) or at zero excursion (which is passed twice per period). Hence the signal should oscillate with twice the vibrational (fundamental) frequency; higher overtones may also be expected. This seems to be a matter of symmetry, and it is not immediately obvious how the symmetry is broken. It does also not help intuition to remember the rule[41] that only those symmetry elements should be invoked, which are common to the minima of lower and upper states. Thus the symmetry group in common to $S_0$ and $S_1$ of ethylene (or of $S_1$ and the ion) is $D_2$, the symmetry of ethylene with intermediate twist angle; but it is not intuitive, how this can render positive and negative torsions of $D_{2h}$ ethylene nonequivalent.

However, these considerations are based on transition probabilities instead of amplitudes. A wave packet is a superposition of stationary wave functions, which includes their relative phase. This phase is generated by the process of preparation. For example, the pump process may prepare the wave packet initially with a phase such that its maximum is on the right in the lower potential, as in Fig. 17. After a time $1/2\nu''$ ($\nu''$ is the vibrational frequency in the lower potential) it would have its maximum on the left, with the phase unchanged. The probe process projects this superposition to a superposition of corresponding vibrational states on the upper potential (frequency $\nu'$), with the same relative phase; the maximum is also on the right hand side (Fig. 17). If $\nu'$ is near zero, *e.g.* as a result of tunneling splitting, this wave function shows practically no time evolution. Since the phase in the lower wave function is time independent after the pumping process and is not changed by the probe, the same upper wave packet (with maximum on the right) would be produced, no matter whether the maximum of the lower function at the time of probing is on the right or left. However, in the example with the tunneling splitting (Fig. 17), the transition probability on the left vanishes.

As a reason for the symmetry breaking one can see the fact that the roles of the pump and probe are not interchangeable. As described, the pump defines the phase, which is then not changed by the probe. One can expect oscillation

 

frequencies only from vibrations of the lower state (populated by the pump). Different phenomena can be expected in one-wavelength experiments, where the identification of pump and probe can be interchanged. In fact, in this case one may observe oscillations in both, the lower and the upper potentials (Section 4.3).

In our mechanism of photodissociation of metal carbonyls, the molecule first relaxes from different initially excited MLCT states to the same repulsive lowest LF surface. (Note that the wave packets arrive at the same $S_1$ surface of the product, although their paths do not exactly coincide there and in the preceding phase.) This seems similar as described by the Kasha rule. However, the relaxation is not vertical. Instead, the molecule is geometrically distorted, the wave packet being controlled by the slopes of the potentials and the internal conversion (MLCT → LF) taking place near a surface crossing. (Control by slopes and intersections is most general for photochemistry, as pointed out in ref. 68.) At first sight, the result seems similar as with the old assumption of vertical internal conversion. In both cases one expects the same products (and we even observed the same oscillations), although there can be differences of lifetimes and appearance times. A certain independence of the initial state was emphasized in our preceding paper.[13] On the other hand, in Section 4.5 we explained by the same mechanism also the wavelength dependence of photolysis observed with many metal carbonyl derivatives. (A wavelength dependence is usually taken as anti-Kasha behavior, if the system is not controlled by conformers or secondary photochemistry.) The crucial feature is the lifetime of the lowest MLCT state (which is not reached from a higher state, because vertical internal conversion is too slow to compete with geometric distortion); it is long, if the barrier (caused by the avoided crossing) is high. If it is long enough for intersystem crossing to occur, the photochemical products will be those of a triplet, while shorter wavelengths give rise to singlet products. Obviously the avoided-crossing model[12] has a high cognitive potential, as it not only rationalizes lifetimes differing by many orders of magnitude (from 12 fs to many nanoseconds or even much more, with triplets taken into account) but also quite a spectrum of phenomena.

This consideration of times reveals a principle that may be more generally important in photochemistry: control by the lifetime or the velocity of motion on the potential surfaces. One can interpret on this basis also, why the excited state ($S_1$) of the product $M(CO)_5$ is reached, although the Jahn–Teller effect distorts the intact molecule already before dissociation in the same direction (CMC bending) that afterwards causes ultrafast $S_1 \rightarrow S_0$ relaxation in the product. Probably the early distortion is not fast enough (because the corresponding slopes are not yet steep enough) to compete with MC stretching (dissociation). On the same basis, and consistent with this interpretation, we can rationalize, why with different pump wavelengths the paths on the LF surface do not coincide: with 350 nm, the wave packet arrives in a valley of the product $S_1$ surface, whereas with 286 nm it arrives near a ridge. It seems that in the latter case the wave packet does not slide fast enough to the valley bottom (along a direction that is again the Jahn–Teller coordinate mentioned). It seems that this principle can also be applied to organic photochemistry, where long excited-state lifetimes facilitate conformer or other isomer equilibration (such as observed in triplet photochemistry), whereas shorter lifetimes (such as those of many but not all singlets) prevent such processes.

## Acknowledgements

This work was supported by the Deutsche Forschungsgemeinschaft (project FU 363/1).

## References

1 M. S. Wrighton, *Chem. Rev.*, 1974, **74**, 401–430.
2 G. L. Geoffroy and M. S. Wrighton, *Organometallic Photochemistry*, Academic Press, New York, 1979.
3 S. A. Mcgregor, O. Eisenstein, M. K. Whittlesey and R. N. Perutz, *J. Chem. Soc., Dalton Trans.*, 1998, 291–300.
4 A. B. Rocha, *J. Phys. Chem. A*, 2007, **111**, 4711–4713.
5 C. Pollak, A. Rosa and E. J. Baerends, *J. Am. Chem. Soc.*, 1997, **119**, 7324–7329.
6 E. J. Baerends and A. Rosa, *Coord. Chem. Rev.*, 1998, **177**, 97–125.
7 A. Rosa, E. J. Baerends, S. J. A. van Gisbergen, E. van Lenthe, J. A. Groeneveld and J. G. Snijders, *J. Am. Chem. Soc.*, 1999, **121**, 10356–11065.
8 K. Pierloot, E. Tsokos and L. G. Vanquickenborne, *J. Phys. Chem.*, 1996, **100**, 16545–16550.
9 N. Ben Amor, S. Villaume, D. Maynau and C. Daniel, *Chem. Phys. Lett.*, 2006, **421**, 378–382.
10 S. Villaume, A. Strich, C. Daniel, S. A. Perera and R. J. Bartlett, *Phys. Chem. Chem. Phys.*, 2007, **9**, 6115–6122.
11 S. A. Trushin, W. Fuß, W. E. Schmid and K. L. Kompa, *J. Phys. Chem. A*, 1998, **102**, 4129–4137.
12 S. A. Trushin, W. Fuß and W. E. Schmid, *Chem. Phys.*, 2000, **259**, 313–330.
13 S. A. Trushin, K. Kosma, W. Fuß and W. E. Schmid, *Chem. Phys.*, 2008, **347**, 309–323.
14 S. A. Trushin, W. Fuß, K. L. Kompa and W. E. Schmid, *J. Phys. Chem. A*, 2000, **104**, 1997–2006.
15 W. Fuß, W. E. Schmid and S. A. Trushin, *J. Phys. Chem. A*, 2001, **105**, 333–339.
16 W. Fuß, S. A. Trushin and W. E. Schmid, *Res. Chem. Intermed.*, 2001, **27**, 447–457.
17 M. J. Paterson, P. A. Hunt, M. A. Robb and O. Takahashi, *J. Phys. Chem. A*, 2002, **106**, 10494–10504.
18 G. A. Worth, G. Welch and M. J. Paterson, *Mol. Phys.*, 2006, **104**, 1095–1105.
19 C. Long, *Top. Organomet. Chem.*, 2010, **29**, 37–71.
20 S. A. Trushin, S. Panja, K. Kosma, W. E. Schmid and W. Fuß, *Appl. Phys. B: Lasers Opt.*, 2005, **80**, 399–403.
21 S. A. Trushin, W. Fuß, K. Kosma and W. E. Schmid, *Appl. Phys. B: Lasers Opt.*, 2006, **85**, 1–5.
22 W. Fuß, S. Panja, W. E. Schmid and S. A. Trushin, *Mol. Phys.*, 2006, **104**, 1133–1143.
23 M. J. Frisch *et al.*, *Gaussian03*, Gaussian Inc., Pittsburgh PA, 2003.
24 P. J. Hay and W. R. Wadt, *J. Chem. Phys.*, 1985, **82**, 270.
25 N. A. Beach and H. B. Gray, *J. Am. Chem. Soc.*, 1968, **90**, 5713–5721.
26 P. Hummel, J. Oxgaard, W. A. Goddard III and H. B. Gray, *Inorg. Chem.*, 2005, **44**, 2454–2458.
27 J. Kim, T. K. Kim, J. Kim, Y. S. Lee and H. Ihee, *J. Phys. Chem. A*, 2007, **111**, 4697–4710.
28 Y. Ishikawa and K. Kawakami, *J. Phys. Chem. A*, 2007, **111**, 9940–9944.
29 V. Jonas and W. Thiel, *J. Chem. Phys.*, 1995, **102**, 8474–8483.
30 J. P. Holland and R. N. Rosenfeld, *J. Chem. Phys.*, 1988, **89**, 7217–7225.
31 J. P. Holland and R. N. Rosenfeld, *Chem. Phys. Lett.*, 1988, **145**, 481–485.
32 W. Fuß, W. E. Schmid and S. A. Trushin, *J. Chem. Phys.*, 2000, **112**, 8347–8362.
33 D. Adelman and D. P. Gerrity, *J. Phys. Chem.*, 1990, **94**, 4055–4060.

34 B. Venkataraman, H. Hou, Z. Zhang, S. Chen, G. Bandukwalla and M. Vernon, *J. Chem. Phys.*, 1990, **92**, 5338–5362.
35 J. J. Turner, J. K. Burdett, R. N. Perutz and M. Poliakoff, *Pure Appl. Chem.*, 1977, **49**, 271–285.
36 J. K. Burdett, J. M. Grzybowski, R. N. Perutz, M. Poliakoff, J. J. Turner and R. F. Turner, *Inorg. Chem.*, 1978, **17**, 147–154.
37 W. C. Trogler, S. E. Desjardin and E. I. Solomon, *Inorg. Chem.*, 1979, **18**, 2131–2136.
38 S.-B. Ko, S.-c. Yu and J. B. Hopkins, *Bull. Korean Chem. Soc.*, 1994, **15**, 762–765.
39 S. A. Trushin, W. Fuß and W. E. Schmid, *J. Phys. B: At., Mol. Opt. Phys.*, 2004, **37**, 3987–4011.
40 A. T. N. Kumar, F. Rosca, A. Widom and P. M. Champion, *J. Chem. Phys.*, 2001, **114**, 701–724.
41 G. Herzberg, *Molecular Spectra and Molecular Structure, Vol. 3: Electronic Spectra and Electronic Structure of Polyatomic Molecules*, Van Nostrand Reinhold, New York, 1966, vol. 3.
42 K. Kosma, S. A. Trushin, W. Fuß and W. E. Schmid, *J. Phys. Chem. A*, 2008, **112**, 7514–7529.
43 S. A. Trushin, S. Sorgues, W. Fuß and W. E. Schmid, *ChemPhysChem*, 2004, **5**, 1389–1397.
44 H. Studzinski, S. Zhang, Y. Wang and F. Temps, *J. Chem. Phys.*, 2008, **128**, 164314/1–164314/10.
45 W. Fuß, W. E. Schmid, K. K. Pushpa, S. A. Trushin and T. Yatsuhashi, *Phys. Chem. Chem. Phys.*, 2007, **9**, 1151–1169.
46 Q. Wang, R. W. Schönlein, L. A. Peteanu, R. A. Mathies and C. V. Shank, *Science*, 1994, **266**, 422–424.
47 A. J. Wurzer, T. Wilhelm, J. Piehl and E. Riedle, *Chem. Phys. Lett.*, 1999, **299**, 296–302.
48 A. J. Wurzer, S. Lochbrunner and E. Riedle, *Appl. Phys. B: Lasers Opt.*, 2000, **71**, 405–409.
49 R. B. Jordan, *Reaction mechanisms of inorganic and organometallic systems*, Oxford Univ. Press, Oxford, 1991.
50 C. Daniel and A. Veillard, *Nouv. J. Chim.*, 1986, **10**, 83–90.
51 H. Hippler, K. Luther, J. Troe and H. J. Wendelken, *J. Chem. Phys.*, 1983, **79**, 239–246 and literature quoted therein.
52 J. Benzler, S. Linkersdörfer and K. Luther, *J. Chem. Phys.*, 1997, **106**, 4992–5005.
53 V. Lehtovuori, P. Myllyperkiö, J. Linnanto, C. Manzoni, D. Polli, G. Cerullo, M. Haukka and J. Korppi-Tommola, *J. Phys. Chem. A*, 2005, **109**, 17538–17544.
54 A. Gabrielsson, M. Towrie and A. Vlček, *Inorg. Chem.*, 2008, **47**, 4236–4242.
55 M. Lezius, V. Blanchet, M. Y. Ivanov and A. Stolow, *J. Chem. Phys.*, 2002, **117**, 1575–1588.
56 H. Harada, S. Shimizu, T. Yatsuhashi, S. Sakabe, Y. Izawa and N. Nakashima, *Chem. Phys. Lett.*, 2001, **342**, 563–570.
57 N. Nakashima, S. Shimizu, T. Yatsuhashi, S. Sakabe and Y. Izawa, *J. Photochem. Photobiol., C*, 2000, **1**, 131–143.
58 A. J. Lees, *Chem. Rev.*, 1987, **87**, 711–743.
59 T. M. McHugh, R. Narayanawamy, A. J. Rest and K. Salisbury, *J. Chem. Soc., Chem. Commun.*, 1979, 208–210.
60 M. S. Wrighton, D. I. Handeli and D. L. Morse, *Inorg. Chem.*, 1976, **15**, 434–440.
61 A. Vlček, *Coord. Chem. Rev.*, 2002, **230**, 225–242.
62 M. A. H. Alamiry, N. M. Boyle, C. M. Brookes, M. W. George, C. Long, P. Portius, M. T. Pryce, K. L. Ronayne, X.-Z. Sun, M. Towrie and K. Q. Vuong, *Organometallics*, 2009, **28**, 1461–1468.
63 A. J. Lees, *Coord. Chem. Rev.*, 2001, **211**, 255–278.
64 S. A. Trushin, T. Yatsuhashi, W. Fuß and W. E. Schmid, *Chem. Phys. Lett.*, 2003, **376**, 282–291.
65 D. Egorova and W. Domcke, *Chem. Phys. Lett.*, 2004, **384**, 157–164.
66 A. Kühl and W. Domcke, *J. Chem. Phys.*, 2002, **116**, 263–274.
67 A. Kühl and W. Domcke, *Chem. Phys.*, 2000, **259**, 227–236.
68 W. Fuß, S. Lochbrunner, A. M. Müller, T. Schikarski, W. E. Schmid and S. A. Trushin, *Chem. Phys.*, 1998, **232**, 161–174.




 